HHS Public Access

Author manuscript

Nat Microbiol. Author manuscript; available in PMC 2021 September 01.

Published in final edited form as:

Nat Microbiol. 2021 April ; 6(4): 435–444. doi:10.1038/s41564-021-00868-1.

Sec24C is an HIV-1 host dependency factor crucial for virus replication

Stephanie V. Rebensburg[1,†], **Guochao Wei**[1,†], **Ross C. Larue**[2], **Jared Lindenberger**[1], **Ashwanth C. Francis**[3], **Arun S. Annamalai**[1], **James Morrison**[1], **Nikoloz Shkriabai**[1], **Szu-Wei Huang**[4], **Vineet KewalRamani**[4], **Eric M. Poeschla**[1], **Gregory B. Melikyan**[3], **Mamuka Kvaratskhelia**[1,*]

[1]Division of Infectious Diseases, University of Colorado Anschutz Medical Campus, Aurora, CO 80045, USA.

[2]College of Pharmacy, The Ohio State University, Columbus, OH 43210, USA.

[3]Department of Pediatrics, Infectious Diseases, Emory University, Atlanta, GA 30322, USA.

[4]Center for Cancer Research, National Cancer Institute, Frederick, MD 21702, USA.

Early events of the HIV-1 lifecycle, such as post-entry virus trafficking, uncoating and nuclear import, are poorly characterized because of limited understanding of virus-host interactions. We used mass spectrometry-based proteomics to delineate cellular binding partners of curved HIV-1 capsid lattices and identified Sec24C as an HIV-1 host dependency factor. Gene deletion and complementation in Jurkat cells revealed that Sec24C facilitates infection and markedly enhances HIV-1 spreading infection. Downregulation of Sec24C in HeLa cells substantially reduced HIV-1 core stability and adversely affected reverse transcription, nuclear import and infectivity. Live cell microscopy showed that Sec24C co-trafficked with HIV-1 cores in the cytoplasm during virus ingress. Biochemical assays demonstrated that Sec24C directly and specifically interacted with hexameric capsid lattices. A 2.3 Å resolution crystal structure of $Sec24C_{228–242}$ in the complex with a capsid hexamer revealed that the Sec24C FG-motif bound to a pocket comprised of two adjoining capsid subunits. Combined with previous data,[1–4] our findings indicate that a capsid-binding FG-motif is conserved in unrelated proteins present in the cytoplasm (Sec24C), the nuclear pore (Nup153[3,4]) and the nucleus (CPSF6[1,2]). We propose that these virus-host interactions during HIV-1 trafficking across different cellular compartments are crucial for productive infection of target cells.

*Correspondence to: mamuka.kvaratskhelia@cuanschutz.edu.
†contributed equally

Author contributions

S.V.R., G.W., R.C.L., J.L., A.C.F., A.S.A., J.M., N.S. and S.W. H. performed the experiments and/or analyzed the experimental results. V.K.R., E.M.P., G.B.M. and M.K. designed and supervised separate sections of the study. M.K. together with S.V.R. and G.W. conceived the entire study and wrote the manuscript with contributions from all other authors.

Competing interests. The authors declare no competing interests.

The HIV-1 core is a macromolecular complex that houses the viral RNA genome and key viral enzymes (reverse transcriptase and integrase) needed for conversion of the single stranded viral RNA into double stranded DNA and its subsequent integration into a host cell chromosome. The outer shell of the native core is composed of about 1,500 capsid (CA) protein monomers, which are arranged predominantly into hexameric lattices, as well as into 12 pentamers, which introduce curvatures at the core periphery to allow assembly of a closed conical structure. A primary role of the CA shell is to protect the virus from immune sensing during early steps of infection[5,6]. At the same time, properly choreographed uncoating of viral cores is essential for reverse transcription and nuclear import[6,7]. The post-entry journey of the core across the cytoplasm and into the nucleus seems to be strongly influenced by interactions of its surface with host cell factors[6,7], but the identity and roles of such factors are poorly deciphered.

To identify cellular proteins that interact with CA we applied a mass spectrometry (MS)-based proteomics approach (Extended Data Fig. 1a) to survey proteins from cellular lysates of THP1 cells with or without interferon (IFN) treatments that co-fractionated with pre-formed WT CA tubes which closely mimic curved hexameric CA lattices in assembled HIV-1 cores[8,9] (Supplementary Tables 1 and 2). Detected hits included known functionally crucial cellular CA binding partners, such as CPSF6[2], Nup153[10], CypA[11,12] and Mx2[13,14] (Supplementary Table 3). As expected[13–16], Mx2 was specifically present in pull-down fractions from IFN treated THP1 cells, whereas IFN treatment did not substantially affect interactions of CypA, Nup153 and CPSF6 with WT CA tubes. These observations with known CA interacting partners provided an initial validation of our experimental approach.

Unexpectedly, annotation of protein hits to their respective cellular compartments and functions revealed co-fractionation of components of the COPII complex with CA tubes[17] (Supplementary Tables 4 and 5). For example, 6 out of 11 proteins of the COPII complex were found in pulled-down fractions, whereas no proteins from the COPI complex were detected. The COPII complex has been extensively studied for its primary role of transporting cargos from the endoplasmic reticulum to the Golgi-apparatus[17], but its individual components might perform additional cellular functions, as they are dispersed throughout the cytoplasm and present in the nuclear pore complex[18].

Sec24C was the top hit among proteins that participate in the COPII complex (Supplementary Table 5). Sec24C was specifically pulled-down in the presence but not in the absence of CA tubes. Furthermore, Sec24C levels were highly enriched (>50-fold) among total cellular proteins co-fractionating with CA tubes compared with its relative abundance in cellular lysate (Supplementary Table 5). Immunoblotting confirmed effective pull-down of endogenous Sec24C from cellular lysates by pre-assembled CA tubes (Extended Data Fig. 1b). IFN treatments had no detectable effect on levels of Sec24C in THP1 cells or its interaction with CA tubes (Extended Data Fig. 1b). Sec24C contains N- (aa 1–314) and C-terminal (aa 315–1094) domains (Fig. 1a). Published functional and structural studies of the C-terminal domain have revealed its interactions with Sec23 (another component of the COPII complex) and various cargo proteins[19]. In contrast, a role for the N-terminal domain has yet to be elucidated.

To examine cellular interactions between Sec24C and HIV-1 cores we used a Trim-fusion based restriction assay[20]. We were able to effectively express the following three fusion proteins: Trim-Sec24C$_{1–196}$, Trim-Sec24C$_{196–314}$ and Trim-Sec24C$_{315–1094}$ (Extended Data Fig. 2a), which collectively covered the entire sequence of Sec24C (Fig. 1a). Trim-Sec24C$_{196–314}$, but not Trim-Sec24C$_{1–196}$ or Trim Sec24C$_{315–1094}$, strongly restricted HIV-1 (Fig. 1b and Supplementary Fig. 1a). Trim-Sec24C$_{196–314}$ also restricted Simian Immunodeficiency Viruses SIVmac239, SIVstm and SIVsmE041, but not Feline Immunodeficiency Virus (FIV), Equine Infectious Anemia Virus (EIAV) or Murine Leukemia Virus (MLV) (Fig. 1c, Extended Data Fig. 2b–h and Supplementary Fig. 1b). These results indicate that Sec24C$_{196–314}$ interacts specifically with primate-lentiviral cores in infected cells.

Searches for sequence similarities between Sec24C$_{196–314}$ and known HIV-1 CA-binding segments[1,3,4,21,22] aligned Sec24C$_{228–242}$ with two known CA binding FG-motifs, CPSF6$_{313–327}$ and Nup153$_{1409–1423}$ (Fig. 1a). Deletion of the Sec24C peptide (Δ228–242) or just its conserved FG amino acids (ΔFG) resulted in loss of the Trim-Sec24C$_{196–314}$ mediated restriction (Fig. 1d). While there are four paralogs of Sec24 (A, B, C and D)[23], the identified CA binding FG-motif is unique to Sec24C. The motif is positioned in an N-terminal region of Sec24C that substantially differs from the other paralogs. To further test significance of the FG-motif for interaction with HIV-1 cores, we compared Sec24C with its closest paralog Sec24D (Extended Data Fig. 3 and 4). Trim-fusion based assays revealed that Sec24C$_{196–314}$ but not its corresponding protein region Sec24D$_{136–256}$ restricted HIV-1 (Extended Data Fig. 3). Complementary biochemical experiments demonstrated that recombinant purified full-length Sec23A/Sec24C heterodimer but not its Sec23A/Sec24D counterpart[24] directly bound to pre-formed CA tubes (Extended Data Fig. 4). Furthermore, the purified FG-motif containing GST-Sec24C$_{196–314}$ bound effectively to pre-assembled WT CA tubes but not to monomeric CA (mCA) protein (Fig. 1e). Neither GST-Sec24C$_{196–314(Δ228–242)}$ nor GST-Sec24C$_{196–314(ΔFG)}$ bound to WT CA tubes (Fig. 1f). Collectively, these results identify the HIV-1 CA-binding FG-motif in Sec24C.

In vitro assembly of purified recombinant CA protein into tubes requires high ionic strength (1.5–2M NaCl) buffers[25]. To determine whether GST-Sec24C$_{196–314}$ could interact with native HIV-1 cores under physiologically relevant buffer conditions, HIV-1 virions were gently lysed with Triton to release viral cores[26]. In a binding buffer containing 100 mM NaCl, GST-Sec24C$_{196–314}$ specifically pulled-down CA from virion lysates (Fig. 1g). Furthermore, GST-Sec24C$_{196–314(ΔFG)}$ failed to bind CA (Fig. 1g). In line with these findings, HIV-1 cores isolated from virion lysates by centrifugation through a linear sucrose gradient (Supplementary Fig. 2) bound to GST-Sec24C$_{196–314}$, but not GST-Sec24C$_{196–314(ΔFG)}$ (Fig. 1h). GST-Sec24C$_{196–314}$ did not bind to monomeric CA (mCA) isolated from the same gradient (Fig. 1h). Collectively, these results show that Sec24C directly binds native HIV-1 cores *in vitro*.

To test whether endogenous Sec24C interacts with incoming HIV-1 cores during early steps of infection, we used a proximity ligation assay (PLA). The results in Figs. 2a–c show that Sec24C associates with HIV-1 (WT CA) and that these interactions are compromised by the N74D CA substitution which is known to impede CA binding to the FG-motifs[1,4].

Consistent with these observations ectopically expressed mCherry-Sec24C preferentially colocalized with IN-mNG labeled HIV-1(WT CA) versus HIV-1(N74D CA) (Extended Data Fig. 5). Next, we performed live cell imaging of ectopically expressed mCherry-Sec24C and the viral complexes containing fluorescent integrase (IN marker HIVeGFP-INmNG)[27,28] in the cytoplasm 1 h post-infection (hpi). The results in Supplementary Video 1 and Fig. 2d reveal stable interaction and co-trafficking of mCherry-Sec24C with HIVeGFP-INmNG labeled complexes. In parallel experiments, co-trafficking was also observed using labeled SNAP-Sec24C and viral cores labeled with the CA marker CypA-DsRed[28] (Supplementary Videos 2 and 3). Together, these findings provide evidence for Sec24C interaction with viral cores in cells during early steps of infection.

To understand how association of Sec24C with viral cores affects HIV-1 infection, we used siRNA-mediated knockdown (KD) of Sec24C in HeLa cells (Extended Data Fig. 6). Sec24C depletion reduced infectivity of HIV-1 (WT CA), but not HIV-1 (N74D CA) (Fig. 2e, Extended Data Fig. 6). Sec24C KD effects on WT HIV-1 were more pronounced in non-dividing vs dividing cells (Extended Data Fig. 6 and Supplementary Fig. 3a) suggesting a significance of Sec24C for effective nuclear import. Analyses of HIV-1 replication intermediates during early steps of infection revealed that viral RNA (Fig. 2f) and p24 (Fig. 2g) levels were comparable in the control and KD cells indicating that Sec24C did not affect the virus entry into infected cells. In contrast, Sec24C depletion reduced levels of cytoplasmic viral cores (~3.2-fold) (Fig. 2h and Supplementary Fig. 3b), reverse transcription (RT) products (~2.8-fold) (Fig. 2i), nuclear pre-integration complexes (~2.6-fold) (Fig. 2j and Supplementary Fig. 3c) and 2-long terminal repeat circles (2-LTRs, a surrogate marker for nuclear import) (~2.0-fold) (Fig. 2k). These effects could be interlinked, as the diminished HIV-1 core stability in Sec24C KD cells seems to proportionally reduce reverse transcription, nuclear import and integration.

Complementary biochemical experiments further investigated effects of GST-Sec24C$_{196–314}$ binding on the stability of isolated native HIV-1 cores and preassembled CA tubes. The results in Extended Data Figs. 7 and 8 show that GST-Sec24C$_{196–314}$ but not GST-Sec24C$_{196–314(\Delta FG)}$ substantially stabilized native cores and pre-formed curved CA lattices. These biochemical observations are in good agreement with the cell-based HIV-1 core stability assay (Fig. 2h and Supplementary Fig. 3b), collectively supporting the stabilizing effect of Sec24C on HIV-1 cores, which, in turn, allows for more effective reverse transcription, nuclear import and infection (Fig. 2).

Next, we investigated whether Sec24C can also affect late steps of HIV-1 replication (Supplementary Fig. 4). Sec24C was not packaged in WT HIV-1 virions, and KD of the protein in virus producer HEK293T cells did not affect virus production or the infectivity of released virions. In accordance with these observations, Trim-Sec24C$_{196–314}$ restricted HIV-1 infection in target HEK293T cells during early steps of infection, whereas the fusion protein had no effect on virus production in HEK293T cells or their infectivity. Taken together, these findings delineate a role for Sec24C during early steps of HIV-1 infection.

To further evaluate a role of Sec24C in HIV-1 replication, we deleted the Sec24C gene through CRISPR-mediated gene knockout (KO) in biologically relevant Jurkat cells and also

re-expressed the WT and ΔFG mutant Sec24C proteins in the KO cells (Supplementary Fig. 5a). Single-round infectivity assays (Extended Data Fig. 9) revealed that Sec24C KO reduced infections of HIV-1, SIVmac239, SIVstm and SIVsmE041 but not FIV, EIAV or MLV. Re-expression of WT but not the ΔFG mutant Sec24C protein in the Sec24C KO cells substantially restored infectivity of the primate lentiviruses. Together with TRIM-based assays (Fig. 1c), these results indicate that Sec24C selectively recognizes incoming cores and facilitates infection of primate lentiviruses.

Next, we assessed involvement of Sec24C in spreading of replication-competent HIV-1 (Fig. 3 and Supplementary Fig. 5b,c). As expected[29,30], HIV-1 robustly replicated in WT Jurkat cells, reaching a maximum at 10 days post infection (dpi). Sec24C KO adversely affected HIV-1 spread over multiple replication cycles, leading to a >100-fold reduction at 10 dpi. Re-expression of WT, but not the ΔFG mutant Sec24C protein in the Sec24C KO cells restored HIV-1 spread to a near WT Jurkat cell level. These findings indicate that Sec24C KO markedly and specifically impairs HIV-1 replication in infected cells.

To understand the structural basis for Sec24C binding to HIV-1 CA, we solved the crystal structure of $Sec24C_{228–242}$ bound to the cross-linked $CA_{A14C/E45C/W184A/M185A}$ hexamer at 2.28 Å resolution (Fig. 4a–b, Supplementary Fig. 6 and Supplementary Table 6). $Sec24C_{228–242}$ engages two adjacent CA subunits with a stoichiometry of six $Sec24C_{228–242}$ molecules bound per CA hexamer. The complex assembly is mediated by the following key interactions: i) Sec24C F236 docks into the deep hydrophobic cavity of CA subunit 2 (colored yellow, Fig. 4a). These observations provide a structural explanation for the site-directed mutagenesis results in Fig. 1d–h, which indicated an essential role of the conserved FG for Sec24C binding to CA in infected cells and *in vitro*; ii) N57 and N74 of CA subunit 2 (colored yellow, Fig. 4b) form 2 hydrogen bonds with the backbone amide and carbonyl of Sec24C F236 and L230, respectively; iii) K182 and Q179 of CA subunit 1 (colored cyan, Fig. 4b) form hydrogen bonds with the backbone carbonyls of Sec24C G233 and P232, respectively.

To test the functional significance of the identified CA interface for binding to Sec24C, we tested relevant CA mutations in infected cells and *in vitro*. The mutant HIV-1 viruses containing N57A and N74D substitutions were fully resistant to Trim-$Sec24C_{196–314}$ (Fig. 4c). In contrast, HIV-1 mutants containing G89V, P90A, A92E and G94D substitutions within and immediately adjacent to the CypA binding loop of CA[21] were fully susceptible to the Trim-$Sec24C_{196–314}$ restriction. Consistent with these cellular assays, purified GST-$Sec24C_{196–314}$ did not bind N57A or N74D CA tubes, but it interacted with G89V, P90A, A92E and G94D CA tubes (Fig. 4d). These structural and functional results also help to explain the specificity of Sec24C for primate lentiviruses (Fig. 1c). For example, HIV-1 CA residues N57 and N74 are conserved in SIVmac239, SIVstm and SIVsm, but not in FIV, EIAV or MLV (Fig. 4e).

The structural results reveal substantial overlap between the $Sec24C_{228–242}$ binding interface on CA and the known interactions of two nuclear proteins CPSF6 and Nup153[1,4] (Extended Data Fig. 10a, b). In particular, key FG residues from Sec24C, CPSF6 and Nup153 dock into the same hydrophobic cavity of CA. In addition, the same cavity is utilized by the small

molecule PF74, which inhibits HIV-1 infection by perturbing uncoating of viral cores, and competing with CPSF6 and Nup153 for their binding to the capsid shell[3,4,31–33] (Extended Data Fig. 10c). Consistent with these structural observations, biochemical assays showed that GST-Sec24C$_{196–314}$ effectively outcompeted cellular CPSF6 and Nup153 binding to CA tubes (Extended Data Fig. 10d,e). Conversely, PF74 inhibited GST-Sec24C$_{196–314}$ binding to HIV-1 cores with an IC_{50} of ~0.692 μM (Extended Data Fig. 10f). Recent reports[34,35] have demonstrated that an experimental long-acting HIV-1 CA inhibitor, GS-6207 (Lenacapavir, Gilead Sciences), targets the same hydrophobic cavity. Therefore, future studies are warranted to elucidate how GS-6207 affects Sec24C interactions with incoming HIV-1 cores in the cytoplasm of infected cells.

The structural information for the FG-motif mediated binding of Sec24C$_{228–242}$ to CA (Fig. 4), together with our proteomics results (Supplementary Table 1), allowed us to search for potential, previously unknown cellular binding partners of HIV-1 CA. Sequence alignment searches among other MS hits (Supplementary Table 1) revealed 9 additional cellular proteins from different cellular compartments with a potential CA binding FG-motif (Supplementary Fig. 7). For further validation we selected cytoplasmic Sec31A (another component of the COPII complex) and nuclear Nup214 (the top nuclear protein hit, Supplementary Table 8). Remarkably, Trim-fusion based assays (Supplementary Fig. 8) reveal that the FG-containing segments of Sec31A and Nup214 selectively recognized HIV-1 in infected cells, whereas they had no effect on MLV infection. Future studies are warranted to test these cellular proteins (Supplementary Fig. 7) for their potential roles in HIV-1 infection.

We have shown that Sec24C is a cytoplasmic host dependency factor for HIV-1 that binds to curved CA lattices via an FG-motif to enable productive infection of target cells. The FG-motif is conserved in seemingly unrelated proteins present in different cellular compartments including cytoplasmic Sec24C, nuclear pore component Nup153[3,4] and nuclear CPSF6[1], and enables virus-host interactions during early steps of HIV-1 replication.

Online Methods

Cells.

HeLa, HEK293T and PhoenixAMPHO cells were cultured in Dulbecco’s modified eagle medium (DMEM, Gibco), 10 % Fetal Bovine Serum (FBS, Sigma-Aldrich) and 1 % Penicillin Streptomycin (Gibco) at 37 °C and 5% CO_2. HeLa cells stably expressing Trim-fusion constructs were generated, as described[20] with the exception of using PhoenixAMPHO instead of HEK293T cells for production of MLV-based particles. Cells stably expressing Trim-fusion constructs were kept under selection pressure in the presence of 1 μg/ml puromycin. THP1, Jurkat and Jurkat derived cells were cultured in Roswell Park Memorial Institute (RPMI) 1640 medium (Gibco) supplemented with 10% FBS and 1% Penicillin-Streptomycin. Live cell numbers in growth curves/analysis were obtained through counting with Trypan-blue exclusion method. For differentiation of THP1, 4×10^6 cells per T175 flask were incubated for 48 hrs with 100 ng/ml PMA with or without 1000 U/ml IFN-α. HEK293T/17 cells (ATCC) and TZM-bl cells (NIH AIDS Reference and Reagent Program) were grown in high-glucose DMEM (Mediatech) supplemented with 10% FBS

(Sigma) and 100 U/ml penicillin-streptomycin (Gemini Bio-Products). The growth medium for HEK293T/17 was supplemented with 0.5 mg/ml G418 sulfate (Mediatech). All cell lines used in the present study were tested monthly using Mycoscope Mycoplasm PCR detection kit and there has been no evidence of *Mycoplasma* contamination.

Derivation and back-complementation of *SEC24C*$^{-/-}$ Jurkat cells.

Jurkat E6–1 cells (ATCC TIB-152) are pseudodiploid with an expected two copies of *SEC24C* on chromosome 10. Alt-R CRISPR-Cas9 tracrRNA (IDT Cat # 1072532), S.p. Cas9 Nuclease 3NLS (IDT Cat # 1074181), Alt-R Cas9 Electoporation Enhancer (IDT Cat # 1075915) were purchased from IDT and used according to the manufacturers instructions. Alt-R CRISPR-Cas9 crRNA specific to SEC24C were synthesized as RNA oligos from IDT.

Pair 1: 5'-AUCAUCAGUCCAGCUAUGGU and 5'-CACAUAAUAUUGCCAGGGUC.

Pair 2: 5'-UGGUUGGGCUGGCUCACUGA and 5'-UCAGGAAGUUUCCCUAACUC.

Pair 1 crRNAs target 82 nt downstream of the ATG for SEC24C and near the stop codon to flank the entire *SEC24C* coding region, while Pair 2 crRNAs target exon 7 and flank the capsid binding peptide. Duplexed crRNA:tracrRNA were formed by incubation of equimolar concentrations of crRNA and tracrRNA to a final concentration of 44 μM. Each pair was then mixed, placed at 95°C for 5 min then allowed to cool to room temperature. Cas9 nuclease was diluted to 36 μM with Resuspension buffer R (Invitrogen Neon transfection kit), then 1 μL of Cas9 nuclease incubated with 1.0 μL of crRNA:tracrRNA duplex for 20 min at room temperature. 5×10^6 Jurkat E6–1 cells in 9 μL of Resuspension buffer R and 2 μL 10.8 μM electroporation enhancer were added the Cas9:crRNA:tracrRNA mixture and loaded into a Neon 10 μL pipette tip. The cells were electroporated using the Neon Transfection System at 1700V for 20ms with 1 pulse, then immediately moved to 2 mL of pre-warmed RPMI. *SEC24C* disruption was determined by PCR amplification of genomic DNA isolated using the Qiagen DNeasy kit. Disruption of *SEC24C* was verified by size-shift of *SEC24C* PCRs, immunoblotting Sec24C from cells and sequencing of the *SEC24C* alleles.

Clones from crRNA pair 1 were first screened with PCR primers located 25kbp apart in wild-type *SEC24C* (5'-GAGATCAAATTGGGAATGCTTTCATAATG and 5'-GCTCCCTACAGAACCATCCAGTGTT) that generate an approximately 513-bp product if the intervening region between the sgRNAs is excised. Of 76 clones screened, 7 yielded the deletion-specific amplicon and were further screened with primers flanking the upstream crRNA targeting sequence and the start codon. This PCR product is expected to be absent from reactions for clones homozygous for *SEC24C* excision, as the reverse primer sits between the crRNA binding sites. All 7 of the clones were positive for this PCR product and the amplicons were sequenced to determine if the open-reading in the remaining non-excised allele was frame-shifted. One clone (clone # 23) was identified with a frameshift of the open reading frame whereas the other 6 clones had only in-frame insertions and deletions of SEC24C.

crRNA pair 2 clones were screened with primers flanking both binding sites (PCR primers 5'-GGCCCACCAACATCGCTGGC and 5'-AGGGCTTGGGATGGCATCAGGG). Wild-type *SEC24C* generates an 833-bp band and a smaller approximately 637-bp amplicon is present if the intervening region between the crRNAs is excised. Of 60 single-cell clones screened for primer pair 2, 14 yielded only bands corresponding to the size of the edited allele. The PCR amplicons were blunt end cloned using the StrataClone Blunt PCR Cloning Kit (Agilent Cat # 240207) and were sequenced from a minimum of five clones to ensure that each allele was sequenced. Five clones were identified to have biallelic frame-shifts of *SEC24C* near the binding peptide. Of these clones, #7 and #9 were analyzed further.

Loss of SEC24C protein expression in clones #23 (from crRNA pair 1), and #7 and #9 (from crRNA pair 2) were verified by immunoblotting. Clone #23 exhibited very similar cell growth rates compared with WT Jurkat cells, whereas clones #7 and #9 exhibited slightly and substantially lower cell growth rates. HIV-1 replication was markedly impaired in all three clones tested. Accordingly, for the present study we used clone #23, which we refer to as Sec24 KO cells. For re-expression of Sec24C(WT) and Sec24C(ΔFG) in Sec24C KO cells lentiviral vectors encoding flag-epitope tagged Sec24C cDNA were used to transduce SEC24C−/− cells. 48 hours post-transduction, cells were selected in 1 μg/mL puromycin. Sec24C(WT) and Sec24C(ΔFG) re-expression was confirmed by immunoblotting.

siRNA mediated knockdown of Sec24C.

The following siRNAs were used for KD experiments: siSec24C (5'-GGCTGCTGTGTAGATCTCT-3') and siCNTRL (silencer negative control siRNA AM4635, Ambion). HeLa and HEK293T cells were transfected through reverse transfection with Lipofectamine RNAiMax (invitrogen), following the manufacturer's instructions, by assembling the siRNA-transfection complexes in the wells of 6-well plates (4 μl RNAiMax and 50–100 pmol siRNA in OptiMEM (Gibco)) at room temperature and then adding 3×10^5 cells to those wells. Where indicated, cells were also treated with 1 μg/ml Aphidicolin 16 hrs before infection. Aphidicolin-treated or-naïve cells were harvested 48 hrs after siRNA transfection and seeded at a density of 5×10^4 cells per well in a 24-well plate, and infections were carried out as described above.

Viral vectors and plasmids.

The following plasmids were used: pNL4–3[36] for replication competent HIV-1; pNL4–3E-R +luc[37] and pHIVscarlet containing WT or mutated (N57A, N74D, G89V, P90A, A92E, G94D) CA coding sequences for a single round HIV-1 infection; SIV based vectors V1eGFP-SIVmac239, V1eGFP-SIVsm041 and V1eGFP-SIVstm37.16[38,39]; FIV based vector pGINSIN[40]; EIAV based vector pEV53[41] and MLV based vectors pMX-RFP[2], pLEGFP[42], pLPCX-Trim(1–299)-HA, pLPCX-Trim(1–299)-CPSF6(261–358)[20]. In addition, we have generated MLV based vectors LPCX-$Trim_{1–299}$-$Sec24C_{1–196}$, pLPCX-$Trim_{1–299}$-$Sec24C_{196–314}$, pLPCX-$Trim_{1–299}$-$Sec24C_{196–314(ΔFG)}$, pLPCX-$Trim_{1–299}$-$Sec24C_{196–314(Δ228–242)}$ and pLPCX-$Trim_{1–299}$-$Sec24C_{315–1094}$. Complementary packaging plasmids included pJK3, pL-VSV-G and pCMV-tat for MLV (MX-RFP virus)[20], pHIT-60 for MLV (eGFP virus)[43], pECX[41] for EIAV and pFP93 [40] for FIV. The VSV-G coding pMD.G[44] was added for pseudotyping of all env-deleted vectors. The pCypA-DsRed and

Vpr-INmNeonGreen (INmNG) plasmids have been described previously[27,28]. The Vpr-INmNeonGreen was constructed by replacing sfGFP with mNeonGeen using BamHI and NotI enzymes (NEB). The pHIV-eGFP (NL4.3 R-E-eGFP) and N74D-eGFP plasmids were a gift from Dr. Christopher Aiken (Vanderbilt University).

Virus stocks.

VSV-G pseudotyped viruses HIV-1, SIVmac239, SIVstm, SIVsmE041, EIAV, FIV, MLV were produced by transfecting respective plasmids into HEK293T or HEK293T/17 cells (seeded at concentrations of 2–4 × 10^5 cells per ml) with X-treme Gene HP (Roche) or JetPrime Transfection reagent (VWR) as described[38,41,45]. Specifically, the cells were transfected with the following plasmids: (pNL4–3E-R+luc or pHIVscarlet or pHIV-eGFP (NL4.3 R-E-eGFP), pMD.G) for HIV-1,; (pEV53, pECX, pMD.G) for EIAV; (pGINSIN, pFP93, pMD.G) for FIV; (pLEGFP, pHIT-60, pMD.G) for MLV; (V1eGFP-SIVmac239, pMD.G) for SIVmac239; (V1eGFP-SIVstm37.16, pMD.G) for SIVstm; and (V1eGFP-SIVsm041, pMD.G) for SIVsmE041. The replication competent HIV-1 was made from the pNL4–3 plasmid. The medium was removed and replaced with fresh medium at 12–16 h post-transfection. The virus containing supernatant was harvested at 72 h post-transfection, clarified, filtered through 0.45-μm-pore-size filter and stored at −80°C.

Trim-based restriction assays.

To probe intracellular interactions between the proteins of interest and incoming HIV-1 cores, we have engineered artificial Trim-fusion constructs. Ectopic expression of the full-length rhTrim5α in human cell lines allows to effectively restrict HIV-1 infection in the cytoplasm[46]. The N-terminal RING, B-box 2, and coiled coil (RBCC) effector domains are responsible for recruiting the proteasomal machinery, whereas C-terminal SPRY domain tethers rhTrim5α to HIV-1 CA. This activity can be maintained in the fusion-proteins if the C-terminal CA binding SPRY domain is replaced by another direct CA interacting partner[3,20]. Accordingly, in the present study we fused indicated segments of Sec24C, Sec31A and Nup214 to the N-terminal part of rhTrim5α. Target cells HeLa, HEK293T and HeLa or HEK293T cells expressing the different Trim-fusion constructs were seeded at a density of 5 × 10^4 cells per well in 500 μl medium in 24-well plates. Five hrs after seeding, the cells were infected with VSV-G pseudotyped viral vectors at various MOIs in the presence of 8 μg/ml polybrene.

Infections.

Infections of WT, Sec24C KO, KO+Sec24C(WT) and KO+Sec24(ΔFG) Jurkat cells were carried out as follows: 1 × 10^6 cells per ml in 1 ml per well of a 12-well plate were infected with 0.25 to 100 ng of HIV-$1_{NL4–3}$ replication competent virus in the presence of 8 μg/ml polybrene for 4 hrs. After washing with PBS, the cells were re-suspended in 1 ml culture medium and cultured for 48 hrs. The supernatant was harvested at each indicated time point, the cells were re-suspended in 1 ml of fresh medium and counted with Trypan blue exclusion staining for live cells. WT, Sec24C KO, KO+Sec24C(WT) and KO+Sec24C(ΔFG) Jurkat cells were split equally at a ratio of about 1:3 at each time point and further cultivated for another 48 hrs. Supernatants harvested at each time point were analyzed with a p24

ELISA (Zeptometrix). Infections of target cells with viruses expressing scarlet or eGFP were determined by flow cytometry and analyzed using BD FACSDiva software (v 8.0.1).

Post-entry core-stability measurements in infected cells.

A live cell-based assay for HIV-1 core stability was performed, as previously described[27,28]. Briefly, VSV-G pseudotyped HIVeGFP particles co-labeled with INmNeonGreen (INmNG) and CypA-DsRed were used to infect HeLa cells transfected with siSEC24C or siCNTRL siRNA (MOI 0.008). Virus was allowed to bind to 5×10^4 HeLa cells adhered to an eight-well chamber slide (Lab-Tek) by spinoculation for 30 min at 1500 × *g*, 12 °C. Prior to virus binding, cell nuclei were stained for 10 min with 2 μg/ml of Hoechst-33342. The cells were washed twice, virus entry was synchronously initiated by adding pre-warmed live-cell imaging buffer (Invitrogen) supplemented with 10% FBS and followed by incubation in a CO_2 incubator maintained at 37 °C. At 3 h post-infection, the cells were moved to a temperature- and CO_2-controlled microscope stage. Images were acquired on a Zeiss LSM880 laser scanning confocal microscope with a 63x/1.4NA oil-immersion objective using Carl Zeiss MicroImaging Zen software Black Version (2.3 SP1). Images were acquired from 4-neighbouring fields of view 5 minutes before- and after addition of 10 μM Cyclosporin A (CsA, Calbiochem) to discriminate between intact virions and post-fusion cores identified based upon the loss of CypA-DsRed from the cytosolic INmNG puncta. 3D-image series were processed off-line using ICY image analysis software (icy.bioimageanalysis.org)[47]. The number of INmNG and CypA-DsRed puncta in pre- and post-CsA treatment images was determined using the spot detector plugin in ICY. The number of stable (CypA-DsRed-containing) cores residing in the cytoplasm was determined by single particle-based detection of CypA-DsRed loss from INmNG puncta upon CsA addition.

Nuclear import.

Hela cells transfected with siCNTRL and siSec24C siRNA were plated (5×10^4 cells/well) on poly-L-lysine treated 8-well chamber slides (LabTek). VSV-G pseudotyped HIVeGFP viruses labeled with INmNG were used to infect the cells at MOI 1. Prior to virus binding, cell nuclei were stained for 10 min with 2 μg/ml of Hoechst-33342. Infection was synchronized by binding virus to cells through spinoculation for 30 min at 1500 × *g*, 12 °C. The cells were washed twice, virus entry was synchronously initiated by adding pre-warmed Fluorobrite medium (GIBCO) supplemented with 10% FBS and followed by culture in a CO_2 incubator. At 4 hrs post-infection, cells were examined under a Zeiss LSM880 laser scanning confocal microscopes using a 63x/1.4NA oil-immersion objective for nuclear HIV-1 complexes. Z-stack images spaced by 0.5 μm were acquired from 4 fields of view. The number of INmNG puncta in the nuclei was determined off-line using ICY software. After image acquisition, the cells were moved back into the cell culture incubator for additional 20 hours. At 24 hours post infection, the cells were fixed with 2% PFA for 7 min. The infected cells from 4 fields of view (~300–400 cells/field) were imaged using a 10x air objective. The fraction of eGFP expressing cells per field of view was determined by normalizing to the total number cells identified by Hoechst-33342 nuclear stain.

PLA assay.

Hela cells (10^5) were seeded on coverslips in 6-well dish. Cells were challenged with VSV-G pseudotyped HIV-1 (MOI=10). Cells were washed and supplied with fresh medium at 1 hpi. Cells were fixed with 4% paraformaldehyde for 15 min at 3 hpi and permeabilized with 0.1% Triton X-100 for 15 min at room temperature. After blocking, cells were incubated with anti-HIV-1 p24 monoclonal antibody (AG 3.0, NIH AIDS Reagent Program) at 1:100 dilution and anti-Sec24C antibody (ab122633, abcam) at 1:50 dilution for 1 h at room temperature. Samples were processed further using a Duolink In Situ Red kit (DUO92101, Sigma-Aldrich) following the manufacturer instructions. Signals were detected by using Olympus FV1000 confocal microscope.

Live-cell imaging.

TZM-bl cells transiently expressing mCherry-Sec24C fusion protein were infected with INmNG-labeled HIVeGFP pseudoviruses. Live-cell imaging of single virus co-trafficking with Sec24C was performed using a Zeiss LSM880 confocal microscope at 37 °C, 5% CO_2. Time-lapse images were collected every 20 or 30 s for a period of 45 min using Z-stacks spaced at 1 μm and covering the cellular volume. Time-lapse movies were processed offline using the ICY image analysis software.

Quantitative analyses of HIV-1 replication intermediates.

HIV-1 RNA levels were analyzed by RT-qPCR, as described[48,49]. Briefly, VSV-G pseudotyped virions produced from HEK293T cells were quantified by HIV-1 P24 ELISA (ZeptoMetrix) and treated with 60 U/ml DNase I (Ambion) to remove the residual plasmid. Hela cells (2×10^5) were infected with VSV-G pseudotyped HIV virions (500 ng of p24) followed by incubation, first on ice for 15 min, and then at 37 °C for 2 h. The cells were washed with PBS four times and then treated with 0.25 % trypsin to remove the unbound virus. Trypsin was inactivated by adding culture medium containing 10% FBS, and the cells were subsequently washed 3 times. RNA was isolated by using RNeasy Mini Kit (Qiagen). Quantification of viral RNA was performed by using reverse transcription and real-time PCR of conserved sequences within *gag*, as described[49]. Quantification of HIV-1 RT products and 2-LTR circles was performed using q-PCR. The primers and qPCR conditions were described previously[50]. Briefly, VSV-G pseudotyped HIV-1 virions produced from HEK293T cells were quantified by HIV-1 p24 ELISA (ZeptoMetrix) and treated with 60 U/ml DNase I (Ambion) to remove the residual plasmid. HeLa cells (2×10^5) were infected with VSV-G pseudotyped HIV-1 virions (500 ng of p24). The cells were collected at 12 hpi. Genomic DNA was isolated by using DNeasy Blood&Tissue kit (Qiagen). All the samples were normalized to GAPDH and $2^{-\Delta\Delta Ct}$ method was used for relative quantification analysis[51].

Immunoblotting.

The following antibodies were used to detect Sec24C (ab122633, Abcam) (1:1000 dilution), Sec24D (A304–813A, Bethyl) (1:1000 dilution), CPSF6 (ab175237, Abcam) (1:1000 dilution), Nup153 (ab24700, Abcam) (1:1000 dilution), Trim5α (ab109709, Abcam)(1:1000

dilution), CD4 (ab133616, Abcam) (1:1000 dilution), Clathrin Heavy Chain (610499, BD Laboratories) (1:1000) and GAPDH (sc-32233, SantaCruz) (1:3000 dilution).

Recombinant proteins.

WT and mutant CA proteins were expressed from pET3a-CA in *E. coli* and purified as described[52]. The quadruple CA mutant for hexamer formation was expressed from pET15b-His-$CA_{A14C/E45C/W184A/M185A}$ and purified as described[53]. For preparation of all GST fused proteins the coding sequences of indicated protein constructs were engineered in the pEX plasmid. The recombinant proteins were expressed in *E. coli* and purified through two column chromatography steps using 5 ml GSTrap 4B and HiTrap Q High Performance 5 ml columns (GE Healthcare). Point-mutations and amino acid deletions in the protein of interest were introduced *via* site-directed mutagenesis (Quickchange II XL site-directed mutagenesis kit, Agilent). Recombinant Sec23A/Sec24C and Sec23A/Sec24D proteins[24] were a gift from Robert Lesch, University of California Berkeley. Protein concentrations were analyzed by using Enspire manager (3.10.3005.1440).

Mass spectrometry.

WT CA tubes were assembled in 50 mM Tris-HCl, pH 8.0, 2 M NaCl overnight at 4 °C. The mixture was centrifuged for 5 min at 21,000 x g, the supernatant was removed and the pelleted CA tubes were used for binding to cellular proteins. THP1 cells were lysed using Passive Lysis Buffer (Promega cat.# E1910) supplemented with protease inhibitors (SIGMAFAST™ Protease Inhibitor Tablets). The ionic strength of the lysate was adjusted to 2 M NaCl by adding 5 M NaCl solutions gradually. The cellular lysate was centrifuged for 2 min at 13,000 x g at 4°C. The obtained supernatant (~100 µl) was added to preformed CA tube pellets. After rotation for 30 min at 4 °C the mixture was centrifuged for 2 min at 13,000 x g. The pellet was washed three times by the assembly buffer 50 mM Tris-HCl, pH 8.0, 2 M NaCl. The remaining pellet was denatured in NuPAGE™ LDS Sample Buffer by boiling and then subjected to SDS-PAGE. The entire lanes were cut out and sliced into ~0.5 cm bands from top to bottom. Each gel piece was transferred to a separate 1.5 ml Eppendorf LoBind tube, distained with 50 % acetonitrile and subjected to in-gel proteolysis using Sequencing Grade Modified Trypsin (Promega V5111) in 50 mM ammonium bicarbonate.

The digested peptides were desalted on a C18 stop-and-go-extraction tips (StageTips). StageTips were prepared by punching 3M Empore C18 material with a Hamilton 20-gauge needle and inserting the disk into P200 pipet tips. StageTips were conditioned with 200 µL of 80 % acetonitrile in 0.1 % formic acid, then centrifuged for 1 min at 1,500 x g. The StageTips were then washed with 200 µL 0.1 % formic acid, and transferred to clean microfuge tubes. The samples were resuspended in 0.1 % formic acid and vortexed for 15 min. The samples were then added to equilibrated C18 columns and centrifuged for 1 min at 1,500 x g. The flow-through was reapplied to the resin three additional times to maximize sample binding. The StageTips were washed twice with 200 µl of 0.1% formic acid and centrifuged at 1,500 x g for 1 min. The StageTips were transferred to a clean micro-centrifuge tube and subjected to two rounds of elution with 100 µL of 0.1 % formic acid in 80 % acetonitrile followed by centrifugation at 1,500 x g. The eluent volume was reduced to

near dryness via Speedvac, then resuspended with 20 μL of 0.1 % formic acid for LC-MS analysis.

Samples were analyzed on an Orbitrap Fusion mass spectrometer (Thermo Fisher Scientific) coupled to an Easy-nLC 1200 system (Thermo Fisher Scientific) through a nanoelectrospray ion source. Peptides were separated on a self-made C18 analytical column (100 μm internal diameter x 20 cm length) packed with 2.7 μm Cortecs particles. After equilibration with 3 μl 5 % acetonitrile 0.1 % formic acid, the peptides were separated by a 70 min a linear gradient from 6 to 38 % acetonitrile with 0.1 % formic acid at 400 nl/min. LC mobile phase solvents and sample dilutions used 0.1 % formic acid in water (Buffer A) and 0.1 % formic acid in 80 % acetonitrile (Buffer B) (Optima™ LC/MS, Fisher Scientific, Pittsburgh, PA).

Data acquisition was performed using the instrument supplied Xcalibur™ (version 4.1) software. Survey scans covering the mass range of 350–1800 were performed in the Orbitrap by scanning from *m/z* 300–1800 with a resolution of 120,000 (at *m/z* 200), an S-Lens RF Level of 30%, a maximum injection time of 50 ms, and an automatic gain control (AGC) target value of 4e5. For MS2 scan triggering, monoisotopic precursor selection was enabled, charge state filtering was limited to 2–7, an intensity threshold of 2e4 was employed, and dynamic exclusion of previously selected masses was enabled for 45 sec with a tolerance of 10 ppm. MS2 scans were acquired in the Orbitrap mode with a maximum injection time of 35 ms, quadrupole isolation, an isolation window of 1.6 m/z, HCD collision energy of 30 %, and an AGC target value of 5e4.

MS/MS spectra were extracted from raw data files and converted into mgf files using a Proteome Discoverer Software (ver. 2.1.0.62). These .mgf files were then independently searched against human database using a Mascot server (Version 2.6, Matrix Science). Mass tolerances were +/−10 ppm for MS peaks, and +/−25 ppm for MS/MS fragment ions. Trypsin specificity was used allowing for 1 missed cleavage. Met oxidation, protein N-terminal acetylation, and peptide N-terminal pyroglutamic acid formation were allowed as variable modifications. Scaffold (version 4.8, Proteome Software, Portland, OR, USA) was used to validate MS/MS based peptide and protein identifications. Peptide identifications were accepted if they could be established at greater than 95.0 % probability as specified by the Peptide Prophet algorithm. Protein identifications were accepted if they could be established at greater than 99.0 % probability and contained at least two identified unique peptides. The mass spectrometry proteomics data have been deposited to the ProteomeXchange Consortium via the PRIDE[54] partner repository with the dataset identifier PXD020970 and 10.6019/PXD020970.

All protein hits with total spectrum count of two or higher (with an exception of keratin contamination) are reported in Supplementary Table 1. Quantitative values (normalized to total spectra) for all identified proteins hits are reported in Supplementary Table 2 and for select proteins in Supplementary Tables 3, 5 and 7. The normalization process performed by Scaffold involves the following three steps: i) determination of the total number of spectra in each biosample; ii) calculation of the average number of spectra across all biosamples; iii) multiplication of each spectrum count for each protein in each biosample by the average count over the respective biosample's total spectral count. The obtained values are displayed

by selecting Quantitative Value (Normalized Total Spectra) in Scaffold, and shown in Supplementary Table 2. These values indicate the relative abundance of each protein hit in respective biosample. Relative enrichment fold values reported in Supplementary Tables 3, 5 and 7 were determined using quantitative value of each protein and the following equation Enrichment=((THP1+CA pull-down) + (THP1+IFN+CA pull-down))/((THP1 input exp I) + (THP1 input exp II)).

Available literature[55–65] and the Human Protein Atlas (www.proteinatlas.org) were used to assign protein hits to respective cellular complexes, organelles and cellular compartments (Supplementary Table 4).

Isolation and interactions of HIV-1 cores with recombinant GST-Sec24C$_{196–314}$.

Thirty milliliters of HIV-1$_{NL4–3E-R+lucVSV-G}$ particles were concentrated by ultracentrifugation through 5 ml of a 20 % sucrose cushion at 25,000 rpm for 2 hrs at 4 °C. The supernatant was removed and the pellet was resuspended in 400 μl STE buffer (10 mM Tris-HCl, pH 7.4, 100 mM NaCl, 1 mM EDTA) on ice for 2 hrs. Virus particles containing 2 μg p24, as measured by p24 ELISA (Zeptometrix), were lysed with 0.25 % Triton X-100 on ice for 10 min. Virion lysates were either directly used for binding assays or were purified further by a linear sucrose gradient[26] to isolate viral cores. Virion lysates or isolated viral cores were incubated with GST-Sec24C$_{196–314}$ on ice for 20 min, and the bound proteins were captured with 20 μl pre-equilibrated glutathione sepharose 4B beads (GE Healthcare) at 4 °C for 20 min. Unbound proteins were washed from the beads with the STE buffer and the bound proteins were analyzed by p24 ELISA or immunoblotting using anti-HIV-1 p55+p24+p17 antibody (ab63917, Abcam). To evaluate PF74 (PF-3450074) effects on GST-Sec24C$_{196–314}$ binding to viral cores, indicated concentrations of PF74 were pre-incubated with viral cores on ice for 20 min and then 500 nM GST-Sec24C$_{196–314}$ was added to the reaction. The pull-down reactions with glutathione sepharose 4B beads (GE Healthcare) were performed as described above and the bound proteins were analyzed by p24 ELISA. Origin 2019 (9.6) software was used to determine the PF74 IC$_{50}$ value.

In vitro binding assays.

WT CA tubes were assembled by incubating 42.5 μM CA in a buffer containing 25 mM Tris-HCl, pH 8.0 and 2 M NaCl overnight on ice. Indicated amounts of tested recombinant proteins or cellular lysates were added to the preformed CA tubes and incubated for 30 min at 4 °C. The mixtures were centrifuged at 21,000 x g for 15 min at 4 °C. Supernatants were discarded, pellets were washed three times and analyzed by SDS-PAGE. For competition assays, preassembled CA tubes were incubated with ~2-fold excess GST-Sec24C$_{196–314}$ for 30 min and then exposed to HeLa cell lysates. The bound fractions were monitored by pelleting the mixture followed by SDS-PAGE and immunoblotting for CPSF6 (ab175237, Abcam) and Nup153 (ab24700, Abcam). To examine interactions with monomeric CA, 42.5μM CA was incubated with 10.6 μM GST-Sec24C$_{196–314}$ in a buffer containing 25 mM Tris, pH8, 150 mM NaCl for 30 min on ice. Pre-equilibrated GST-beads were used to capture bound proteins. Unbound proteins were washed out from the beads using 25 mM Tris-HCl, pH 8.0, 150 mM NaCl and the bounds proteins were analyzed by SDS-PAGE and visualized by AcquaStain.

To monitor interactions between full-length recombinant Sec23A/Sec24C and Sec23A/Sec24D heterodimers with CA tubes, we used the CA(A92E) protein. The ability of the CA(A92E) mutant protein to effectively assemble into tubes under lower ionic strength (1 M NaCl[9]) compared to WT CA (2 M NaCl) was exploited to avoid background precipitation of Sec23A/Sec24C and Sec23A/Sec24D heterodimers at higher NaCl concentrations. The tubes were assembled with 10 mg/ml CA(A92E) in the buffer containing 50 mM Tris-HCl, pH 7.5, 1 M NaCl at room temperature and then Sec23A/Sec24C and Sec23A/Sec24D heterodimers (0.03 mg/ml) were added to the reaction. After 30 min incubation at room temperature, the mixtures were centrifuged at 21,000 x g. The supernatants were removed and the pellets were washed three times with 50 mM Tris-HCl, pH 7.5, 1 M NaCl, 0.01% NP40, 2% glycerol. The remaining pellets were dissolved in 100 μl of NuPAGE™ LDS Sample Buffer by boiling and subjected to SDS-PAGE analysis. The control runs were conducted under identical conditions except the CA(A92E) protein was omitted from the reactions.

Stability of isolated native cores *in vitro*.

Single HIV-1 particles labeled with INsfGFP were bound to a poly-L-lysine treated cover glass and mildly permeabilized with saponin (100 μg/ml) for 1 min. Saponin was washed away, and recombinant purified proteins GST-Sec24C$_{196–314}$, GST-Sec24C$_{196–314(\Delta FG)}$ or buffer (dPBS+150mM NaCl) were added to the permeabilized virions, incubated at 37 °C for 10 min and fixed with 2% PFA (10 min). In parallel samples, the permeabilized virions were fixed without further incubation to serve as controls. After PFA fixation, the cores were co-incubated for 1 min with 100 nM of recombinant CypA-DsRed that readily binds to mature viral cores, but not immature Gag/Gag-Pol polyproteins. This enabled the identification of mature cores bound on glass. Unbound CypA-DsRed was washed off, and confocal images were acquired from 4 neighboring fields of view. The number of CypA-DsRed-positive INmNG labeled cores after 10 min incubation at 37 °C was quantified by ICY image analysis software[66] and normalized to the total number of cores detected at 0 min.

Stability of CA tubes.

Preassembled CA tubes (see above) were incubated with GST-Sec24C$_{196–314}$, GST-Sec24C$_{196–314(\Delta FG)}$ or buffer for 30 min and then reaction mixtures were centrifuged at 21,000 x g for 15 min at 4 °C. Supernatants were discarded and pellets were re-suspended in a buffer containing 1 M NaCl, 25 mM Tris-HCl, pH 8.0 and 1 M NaCl, and incubated on ice for 0, 7.5, 15, 30, 60, 90 or 120 min. The samples from each time point were centrifuged for 5 min at 21,000 x g at 4 °C and resulting pellets were analyzed by SDS-PAGE and AcquaStain.

X-ray crystallography.

The inter-subunit disulfide-stabilized CA$_{A14C/E45C/W184A/M185A}$ hexamers were prepared as described[53]. Assembled hexamers were further purified *via* size exclusion chromatography using a GE Healthcare HiLoad 16/600 Superdex 200 pg column and a buffer containing 20 mM Tris-HCl, pH 8.0 and 150 mM NaCl. CA$_{A14C/E45C/W184A/M185A}$ hexamers were detected using non-reducing SDS-PAGE and concentrated to 30 mg/mL with a 50 k cutoff

Amicon Ultra-15 Centrifugal concentrator. The $Sec24C_{228–242}$ peptide was synthesized by Biomatik. Pre-formed $CA_{A14C/E45C/W184A/M185A}$ hexamer (17.8 mg/mL) was mixed with 4 mM synthetic $Sec24C_{228–242}$ peptide to form the complex. The equal volume of a well solution containing 12% PEG3350, 0.35 M NaI, 0.1 M sodium cacodylate pH 6.5, and 24% glycerol was added to the complex mixture and crystals were grown at 4°C in hanging drop well format. Conical shaped crystals appeared within one week. Crystals were flash-cooled in liquid nitrogen and data were collected at the Advanced Light Source, Beamline 5.0.1 at 100 K and a wavelength of 0.97741 Å. All data were processed and scaled using XDS[67]. Phaser[68] in the PHENIX suite[69] was used to perform molecular replacement using PDB 4U0A as a search model. Phenix.refine[70] was used for data refinement, and manual refinement was done in Coot[71]. Final Ramachandran statistics are 97% favorable, 2% allowed. The coordinates are deposited in the Protein Data Bank under accession codes 6PU1.

Statistical analyses.

Statistical analysis of samples was done with Student's two-sample, two tailed *t*-test.

Extended Data

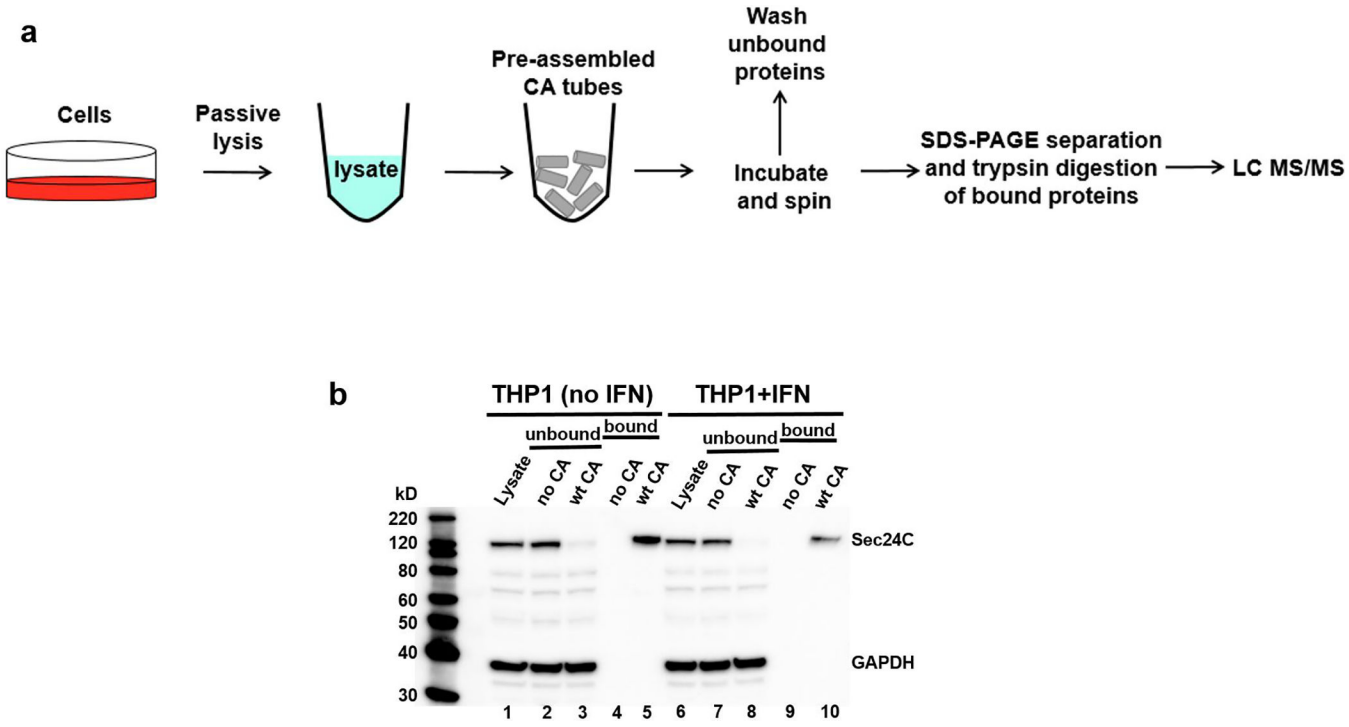

Extended Data Fig. 1. Identification of Sec24C as HIV-1 CA interacting partner.

(a) Experimental design of the MS-based proteomics approach (See Online Methods for details). (b) Representative immunoblots showing CA tubes mediated pull-downs of endogenous Sec24C from THP1 cells without (lanes 1–5) or with (lanes 6–10) IFN treatments. Lanes 1 and 6: lysates, 2 and 7: supernatant or unbound fraction after pull-down in the absence of CA tubes, 3 and 8: supernatant or unbound fraction after pull-down in the

presence of CA tubes; 4 and 9: pelleted or bound fraction in the absence of CA tubes; 5 and 10: pelleted or bound fraction in the presence of CA tubes.

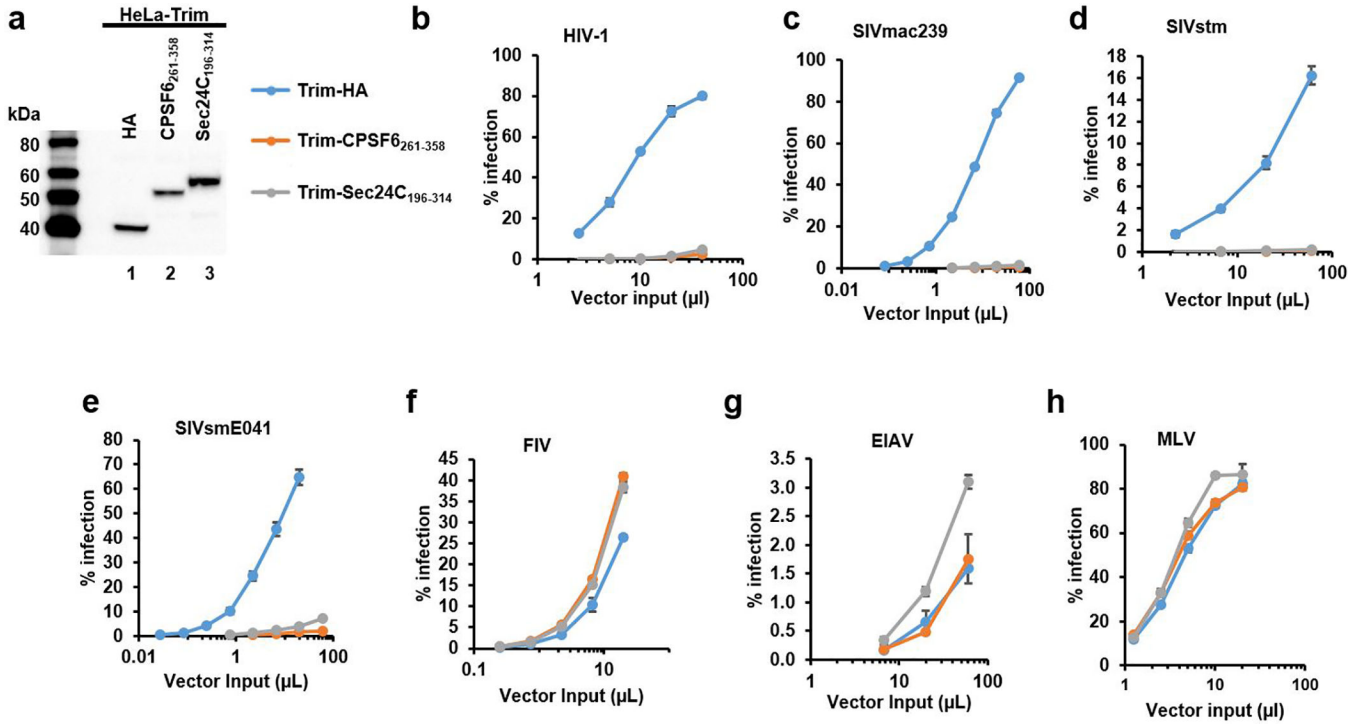

Extended Data Fig. 2. Effects of Trim-Sec24C$_{196–314}$ on different retroviruses.

(a) Representative immunoblot showing the stable expression of Trim-HA (blue line), Trim-CPSF6$_{261–358}$ (orange line) and Trim- Sec24C$_{196–314}$ (gray line) in HeLa cells. (b-h) Infections of HeLa cells stably expressing indicated Trim-fusion constructs with following VSV-G pseudotyped viruses: HIV-1NL4–3 (b), SIVmac239 (c), SIVstm (d), SIVsmE041 (e), FIV (f), EIAV (g), MLV (h). Infection levels of HIV-1-scarlet, SIVstm-eGFP, SIVmac239- eGFP, SIVsmE041-eGFP, FIV-eGFP, EIAV-eGFP, and MLV-RFP were determined by fluorescence- activated cell sorting (FACS). The averaged data (mean values +/− SD) from three independent experiments are shown with exception of FIV infection in Trim-HA overexpressing and EIAV infection in Trim-CPSF6$_{261–358}$ overexpressing Hela cells which were obtained from two independent experiments.

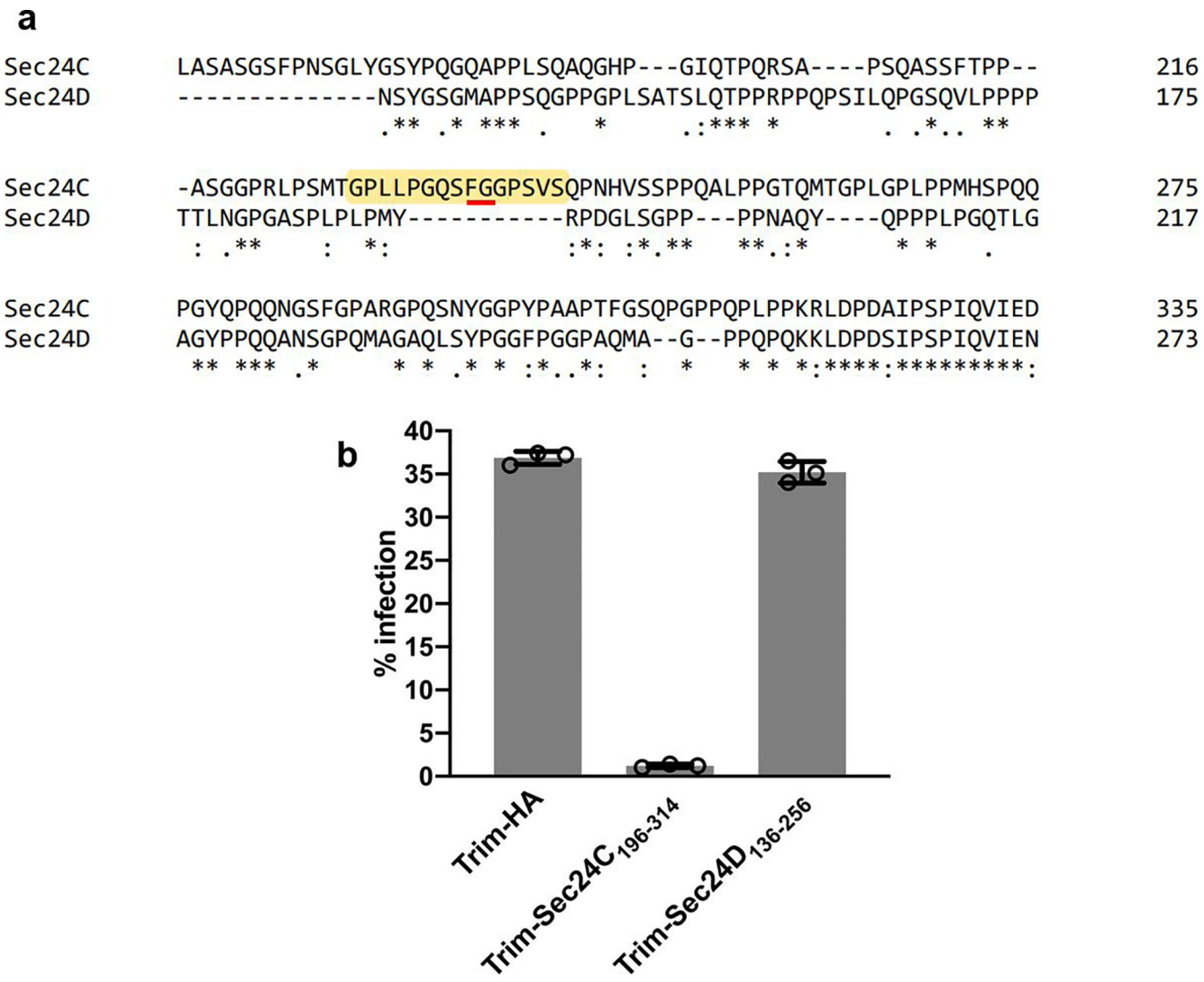

Extended Data Fig. 3. Comparative analysis of corresponding protein regions from Sec24C and Sec24D.

(a) Sequence alignment of corresponding N-terminal regions of Sec24C and Sec24D are shown. The full-length proteins (NCBI ref sequences: NP_004913.2 and NP_055637.2) were aligned using Clustal Omega program from EMBL-EBI. The CA binding FG-motif in Sec24C is highlighted in yellow and the FG residues are underlined with red. (b) Effects of stably expressing Trim-Sec24C$_{196–314}$ and Trim-Sec24D$_{136–256}$ on HIV-1 infection in HeLa cells. The data (mean values +/− SD) from three independent experiments are shown.

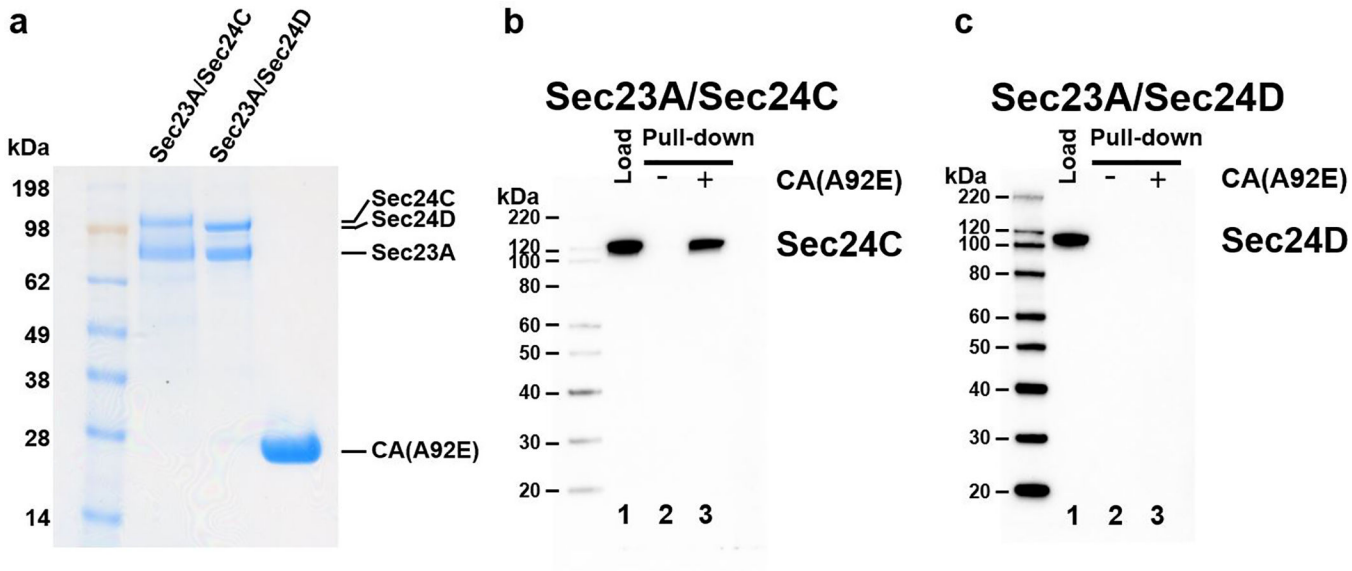

Extended Data Fig. 4. Comparative analysis of full-length Sec23A/Sec24C and Sec23A/Sec24D for their interactions with CA tubes *in vitro*.

Interactions of purified recombinant Sec23A/Sec24C and Sec23A/Sec24D heterodimers with preassembled HIV-1 CA(A92E) tubes were analyzed. Since Sec23A/Sec24C and Sec23A/Sec24D heterodimers were not sufficiently soluble in a 2 M NaCl containing buffer needed for assembly WT CA tubes, we used CA(A92E) which allowed us to effectively assemble the tubes with 1 M NaCl. In turn, the lower ionic strength conditions enabled us to avoid a background precipitation of the Sec23A/Sec24C and Sec23A/Sec24D heterodimers. (a) A representative SDS-PAGE image of stock solutions of Sec23A/Sec24C, Sec23A/Sec24D and CA(A92E) proteins visualized by BlueFast Protein Staining Solution. (b-c) Representative immunoblotting images of Sec23A/Sec24C (b) and Sec23A/Sec24D (c) interactions with CA(A92E) tubes. The Sec23A/Sec24C and Sec23A/Sec24D heterodimers were diluted to 0.03 mg/ml for the pull-down assays to avoid background protein precipitation. Lanes 1: load of Sec23A/Sec24C (b) or Sec23A/Sec24D (c); Lanes 2: pull-downs in the absence of CA; Lanes 3: preassembled CA(A92E) tubes were incubated with Sec23A/Sec24C (b) or Sec23A/Sec24D (c) in the assembly buffer. The mixture was centrifuged and washed three times with the buffer containing 50 mM Tris- HCl, pH 7.5, 1 M NaCl, 0.01% NP40, 2% glycerol. The pelleted fractions were run on SDS-PAGE and visualized by Sec24C (b) or Sec24D (c) antibody.

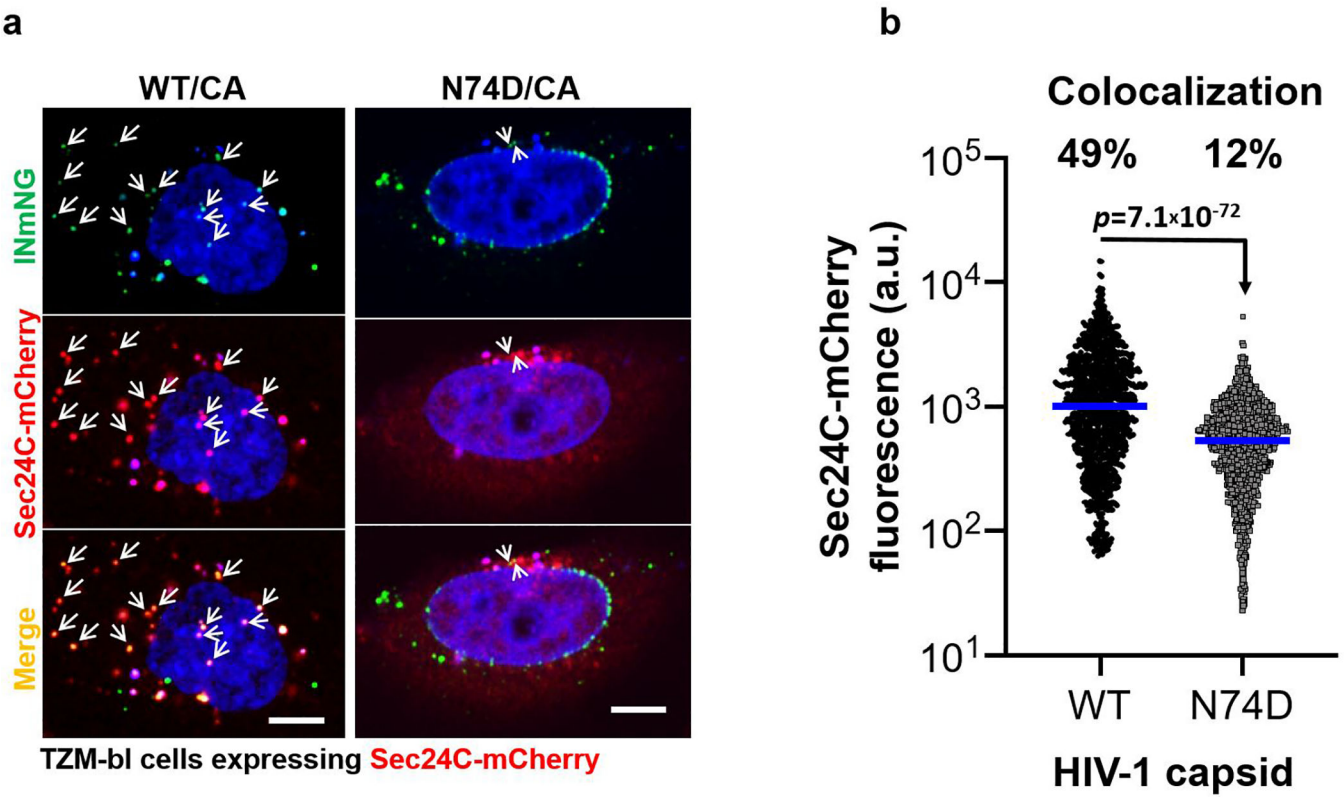

Extended Data Fig. 5. Analysis of cytoplasmic HIV-1 core colocalization with Sec24C.

TZM-bl cells transiently expressing Sec24C-mCherry were infected with INmNG-labeled HIV-1 bearing WT CA or the N74D CA mutant. At 2 hpi, cells were analyzed for colocalization of INmNG-labeled WT or mutant N74D virus with Sec24C. (a) Representative images and (b) quantification of Sec24C-mCherry signal associated with INmNG-labeled puncta. The results are from n=1202 WT/CA puncta from 43 cells and n=1202 N74D/CA puncta from 25 cells. Colocalization (%) of the Sec24C-mCherry signal with INmNG puncta is shown in the graph. The averaged data are representative of two independent experiments. Statistical significance was determined by two-tailed student *t*-test. Arrows in (a) point to Sec24C-mCherry puncta colocalized with INmNG spots. Scale bar is 5 μm.

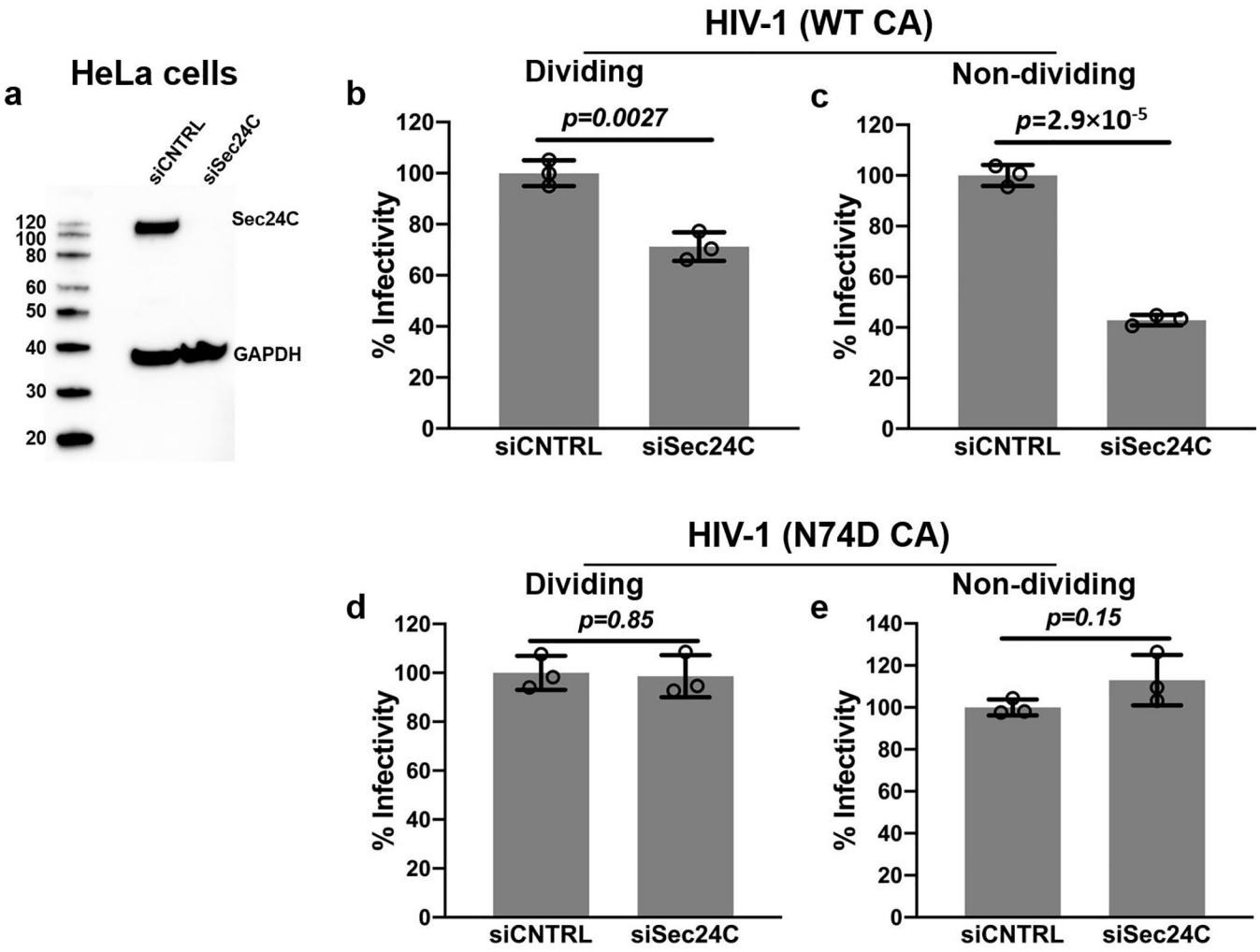

Extended Data Fig. 6. Effects of Sec24C KD on infectivity of HIV-1 (WT CA) and HIV-1 (N74D CA).

(a) Representative immunoblot for the siRNA mediated KD of Sec24C in HeLa cells. (b and c) Infectivity (normalized to negative control KD) of VSV-G pseudotyped HIV-1 virus in WT and Sec24C KD Hela cells without (b) and with (c) 1 μg/ml Aphidicolin. (d-e) Infectivity (normalized to negative control KD) of VSV-G pseudotyped HIV-1 N74D CA mutant virus in WT and Sec24C KD Hela cells without (d) and with (e) 1 μg/ml Aphidicolin. The data (mean values +/− SD) from three independent experiments are shown. Statistical significance was determined by two-tailed student *t*-test.

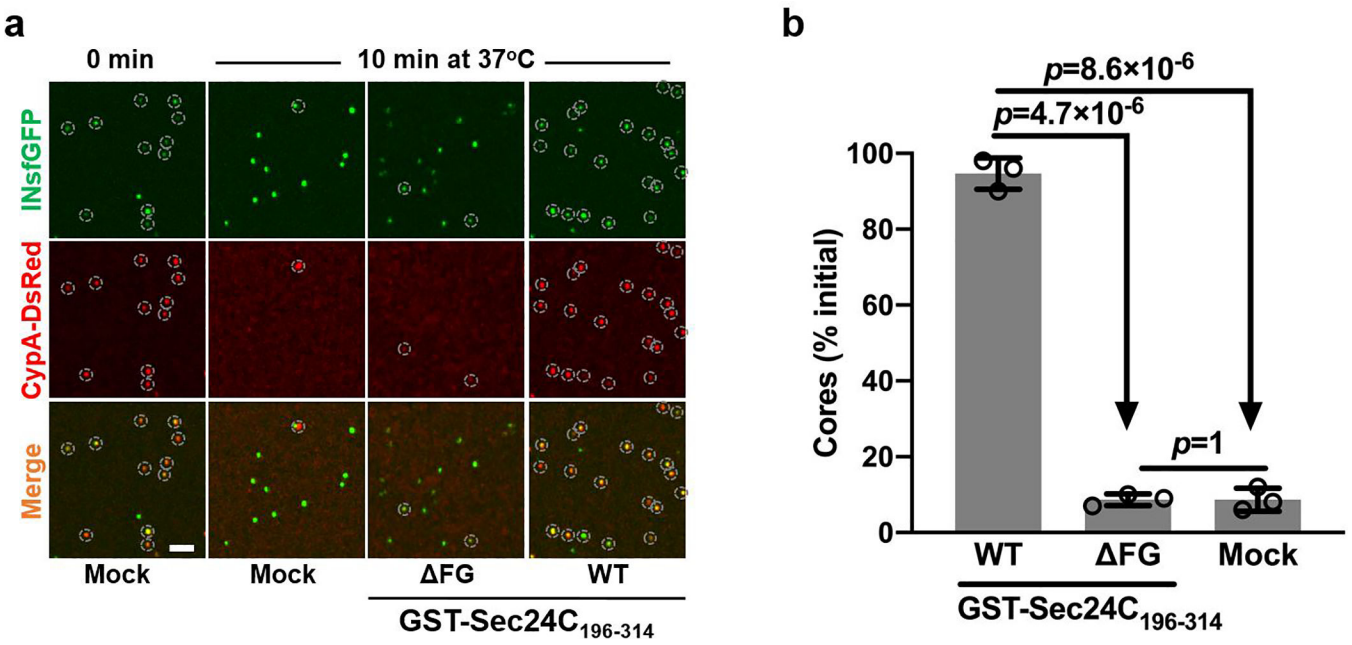

Extended Data Fig. 7. Effects of GST-Sec24C$_{196–314}$ on stability of isolated native HIV-1 cores.

VSV- G pseudotyped HIV-1 particles fluorescently labeled with INmNG (green) were bound to a poly-lysine-coated coverslip and treated with Saponin (100 μg/ml, 1 min) to expose the viral cores. Cores were either fixed immediately after saponin treatment (0 min) or after 10 min incubation at 37 °C with 25 μM of GST- Sec24C$_{196–314}$, GST-Sec24C$_{196–314(\Delta FG)}$ or with buffer (mock). After PFA fixation the cores were incubated with 100 nM of recombinant CypA-DsRed to bind the mature viral cores. (a) Representative images show INmNG and CypA-DsRed labeled HIV-1 cores after 0 and 10 min of incubation in the presence of GST-Sec24C$_{196–314}$, GST-Sec24C$_{196–314(\Delta FG)}$ or buffer. Dashed white circles show INmNG and CypA-DsRed colocalized puncta. Scale bar is 2 μm. (b) The data (mean values +/− SD) from three independent experiments are shown. Statistical significance was determined by two-tailed student *t*-test.

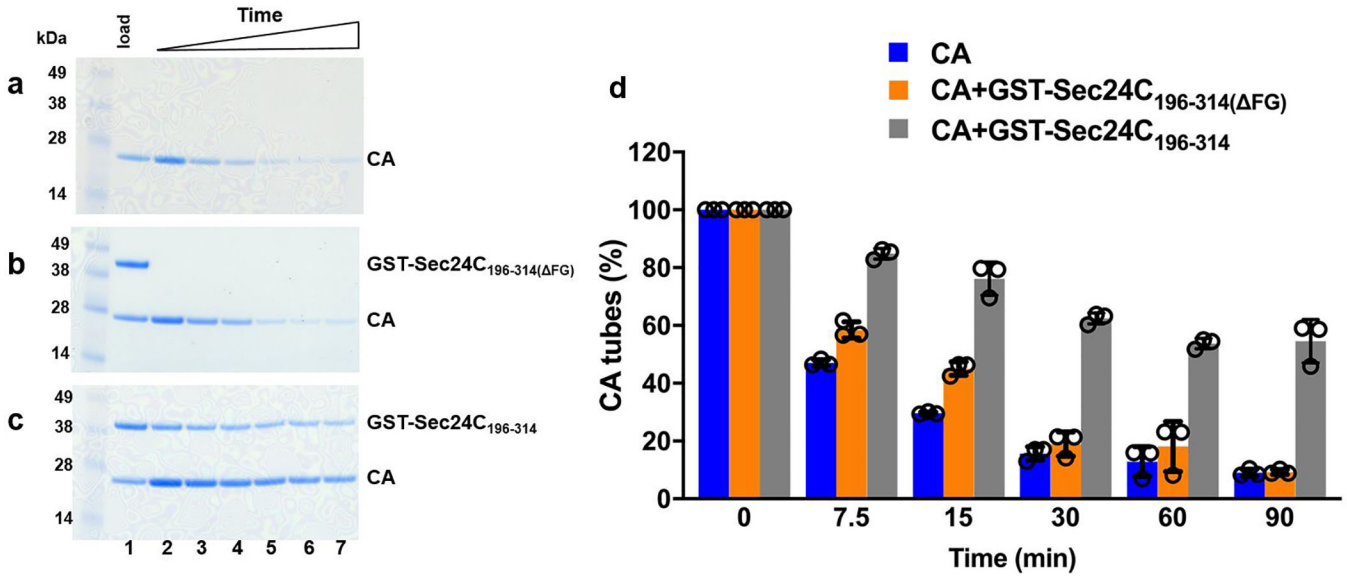

Extended Data Fig. 8. Effects of GST-Sec24C$_{196–314}$ on the stability of CA tubes.

(a-c) Stability of CA tubes as a function of time. CA tubes were pre-formed at 2 M NaCl, pelleted and then re-suspended in a 1 M NaCl containing buffer to induce disassembly of the tubes (a). GST-Sec24C$_{196–314(ΔFG)}$ (b) or GST-Sec24C$_{196–314}$ (c) was added to pre-formed CA tubes and then reactions were diluted to 1 M NaCl buffer. The mixtures were centrifuged at indicated time points and pellets were analyzed by SDS-PAGE. (d) Quantification of the results in (a-c). The data (mean values +/− SD) from three independent experiments are shown.

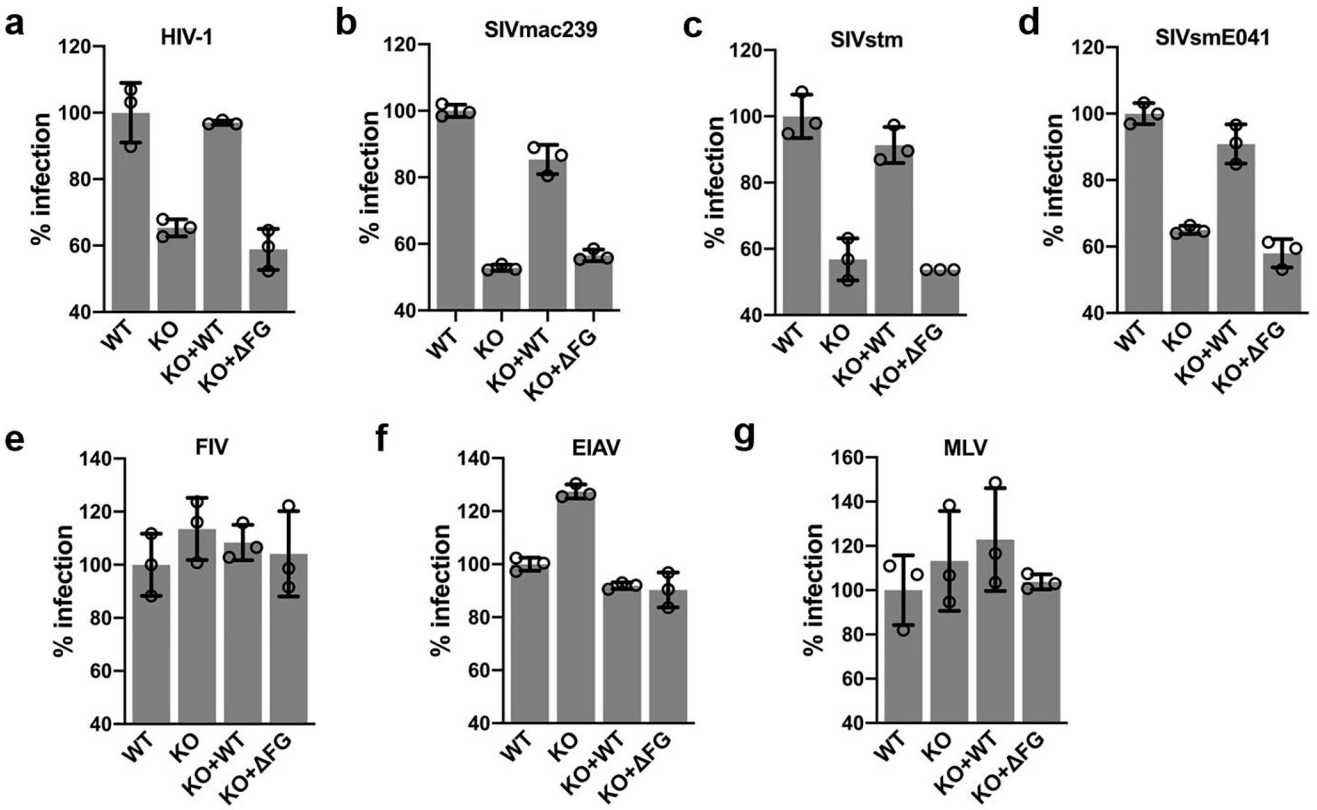

h

	HIV-1	SIVmac239	SIVstm	SIVsmE041	FIV	EIAV	MLV
WT vs KO	0.003	2.4×10^{-6}	0.0012	5.9×10^{-5}	0.230201	0.0002	0.4521
KO vs KO+WT	3.2×10^{-5}	0.0002	0.002	0.0017	0.545583	3.0×10^{-5}	0.6329
KO+WT vs KO+ΔFG	0.0004	0.0004	0.0002	0.001	0.694477	0.7073	0.2309

Extended Data Fig. 9. Effects of Sec24C KO and repletion on infection of different retroviruses.

Single-cycle replication assays were performed in WT, Sec24C KO, KO+Sec24C, or KO +Sec24C(ΔFG) Jurkat cells. Infection levels (normalized to WT Jurkat cells) of VSV-G pseudotyped eGFP reporter viruses: HIV-1 (a), SIVmac239 (b), SIVstm (c), SIVsmE041 (d), FIV (e), EIAV (f), MLV (g) were measured by FACS. The data (mean values +/− SD) from three independent experiments are shown. (h) *P*-values. Statistically significant changes were observed for all lentiviruses, when their infection levels were compared for KO vs WT, KO+WT vs KO and KO+ΔFG vs KO+WT. In contrast, no statistically significant differences were seen for FIV or MLV across these cell lines. Sec24C KO resulted in slight but statistically significant increase of EIAV infection (KO vs WT). This effect is opposite to Sec24C KO effects on primate lentiviruses. Furthermore, in complete contrast with primate lentiviruses, no detectable differences were observed for EIAV in KO+ ΔFG vs KO+WT cells. Statistical significance was determined by two-tailed student *t*-test.

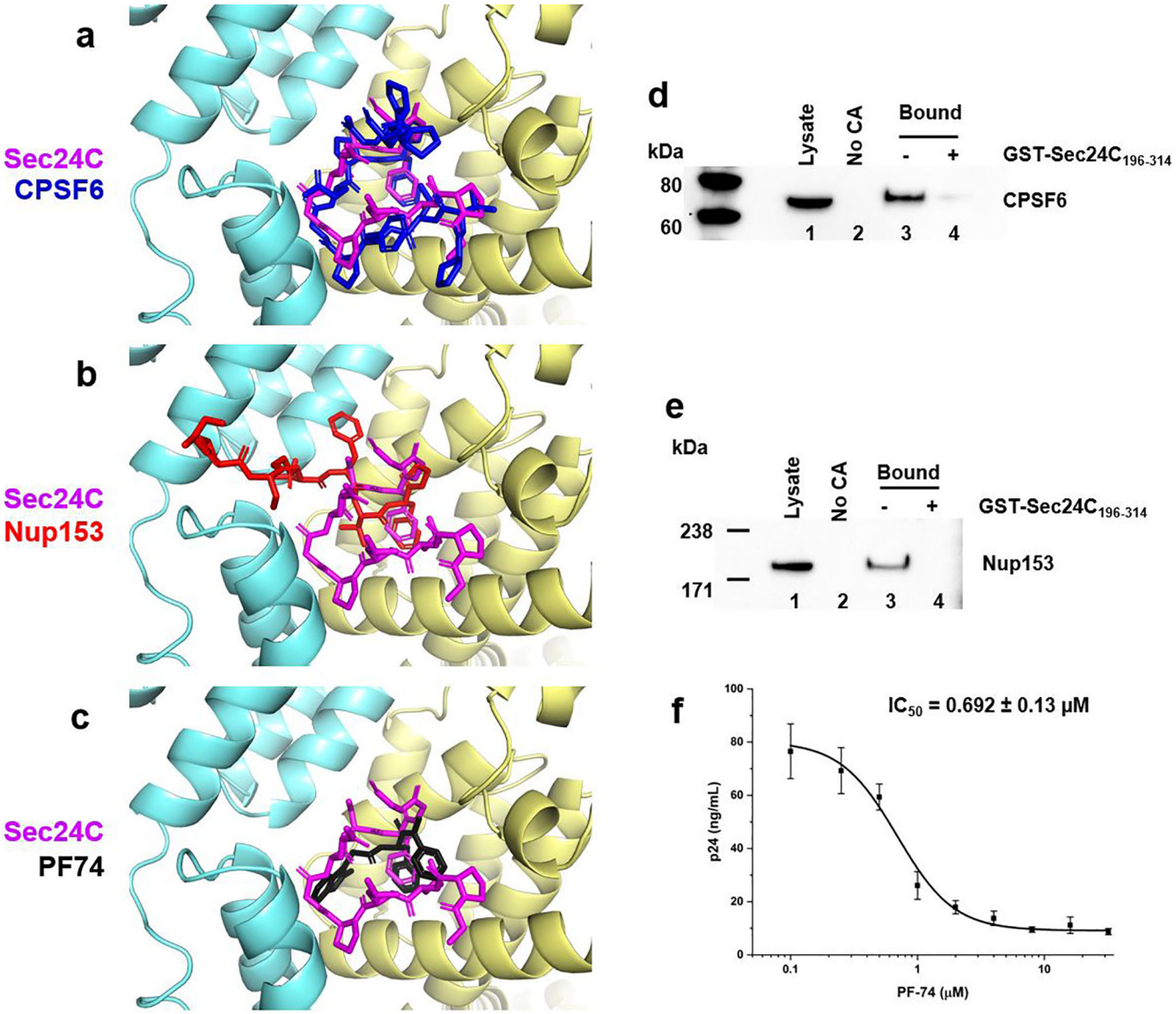

Extended Data Fig. 10. Comparative analyses of interactions of cognate cellular proteins and PF74 inhibitor with CA.

(a-c), Superimposition of the x-ray crystal structures of the Sec24C peptide (magenta) with CPSF6 peptide (blue) (a), Nup153 peptide (red) (b) and PF74 (black) (c) binding sites. (d-f), Competition assays to show CPSF6 (d) and Nup153 (e) pull-downs from HeLa cell-lysates by CA tubes in the absence (lane 3) and presence (lanes 4) of GST-Sec24C$_{196–314}$. Representative immunoblots for CPSF6 and Nup153 are shown for the following samples. Lanes: 1, cellular lysates; 2, pelleting of cellular lysates in the absence of CA tubes; 3, pelleting of cellular lysates with CA tubes; 4, pelleting of cellular lysates with CA tubes + 2-fold excess GST-Sec24C$_{196–314}$. (f), PF74 dose-dependent inhibition of interactions of GST-Sec24C$_{196–314}$ with HIV-1 cores. The data (mean values +/− SD) from three independent experiments are shown. The results were analyzed by Origin 2019 software to determine the IC_{50} value.

Supplementary Material

Refer to Web version on PubMed Central for supplementary material.

Acknowledgments

Purified recombinant Sec23A/Sec24C and Sec23A/Sec24D proteins were a gift from Robert Lesch, University of California Berkeley. We are grateful to Dr. Monika Dzieciatkowska, University of Colorado School of Medicine Biological Mass Spectrometry Facility, for her help with proteomics studies. We thank Paul Bieniasz, the Rockefeller University, for insightful discussions and advice. We are grateful to Pratibha Koneru, Stephanie Bester, KyeongEun Lee, Yuhan Pan and other members of the participating laboratories for their help with data analysis, providing some reagents and valuable suggestions. This work was supported by NIH grants R01 AI062520 and R01 AI157802 (to M.K.), U54 GM103368 (to M.K., A.C.F. and G.B.M.), R01 AI129862 (to G.B.M.), KL2 TR001068 (to R.C.L.), R01 AI77344 (to E.M.P).

Data availability statement

The data sets generated and analyzed during the current study are included in this article or are available in the Protein Data Bank under the accession number 6PU1 (structural data), and via ProteomeXchange with identifier PXD020970 (proteomics data). All other data are available from the corresponding author upon request. Source data are provided with this paper.

References

1. Price AJ et al. CPSF6 defines a conserved capsid interface that modulates HIV-1 replication. PLoS Pathog. 8, e1002896, doi:10.1371/journal.ppat.1002896 (2012). [PubMed: 22956906]
2. Lee K et al. Flexible use of nuclear import pathways by HIV-1. Cell Host Microbe 7, 221–233 (2010). [PubMed: 20227665]
3. Matreyek KA, Yucel SS, Li X & Engelman A Nucleoporin NUP153 phenylalanine-glycine motifs engage a common binding pocket within the HIV-1 capsid protein to mediate lentiviral infectivity. PLoS Pathog 9, e1003693, doi:10.1371/journal.ppat.1003693 (2013). [PubMed: 24130490]
4. Price AJ et al. Host cofactors and pharmacologic ligands share an essential interface in HIV-1 capsid that is lost upon disassembly. PLoS Pathog. 10, e1004459, doi:10.1371/journal.ppat.1004459 (2014). [PubMed: 25356722]
5. Rasaiyaah J et al. HIV-1 evades innate immune recognition through specific cofactor recruitment. Nature 503, 402–405, doi:10.1038/nature12769 (2013). [PubMed: 24196705]
6. Campbell EM & Hope TJ HIV-1 capsid: the multifaceted key player in HIV-1 infection. Nat. Rev. Microbiol. 13, 471–483, doi:10.1038/nrmicro3503 (2015). [PubMed: 26179359]
7. Yamashita M & Engelman AN Capsid-Dependent Host Factors in HIV-1 Infection. Trends Microbiol. 25, 741–755, doi:10.1016/j.tim.2017.04.004 (2017). [PubMed: 28528781]
8. Mattei S, Glass B, Hagen WJ, Krausslich HG & Briggs JA The structure and flexibility of conical HIV-1 capsids determined within intact virions. Science 354, 1434–1437, doi:10.1126/science.aah4972 (2016). [PubMed: 27980210]
9. Zhao G et al. Mature HIV-1 capsid structure by cryo-electron microscopy and all-atom molecular dynamics. Nature 497, 643–646, doi:10.1038/nature12162 (2013). [PubMed: 23719463]
10. Brass AL et al. Identification of host proteins required for HIV infection through a functional genomic screen. Science 319, 921–926 (2008). [PubMed: 18187620]
11. Franke EK, Yuan HE & Luban J Specific incorporation of cyclophilin A into HIV-1 virions. Nature 372, 359–362, doi:10.1038/372359a0 (1994). [PubMed: 7969494]
12. Thali M et al. Functional association of cyclophilin A with HIV-1 virions. Nature 372, 363–365, doi:10.1038/372363a0 (1994). [PubMed: 7969495]

13. Goujon C et al. Human MX2 is an interferon-induced post-entry inhibitor of HIV-1 infection. Nature 502, 559–562, doi:10.1038/nature12542 (2013). [PubMed: 24048477]
14. Kane M et al. MX2 is an interferon-induced inhibitor of HIV-1 infection. Nature 502, 563–566, doi:10.1038/nature12653 (2013). [PubMed: 24121441]
15. Bulli L et al. Complex Interplay between HIV-1 Capsid and MX2-Independent Alpha Interferon-Induced Antiviral Factors. J. Virol. 90, 7469–7480, doi:10.1128/JVI.00458-16 (2016). [PubMed: 27279606]
16. Kane M et al. Nuclear pore heterogeneity influences HIV-1 infection and the antiviral activity of MX2. Elife 7, doi:10.7554/eLife.35738 (2018).
17. Jensen D & Schekman R COPII-mediated vesicle formation at a glance. J. Cell Sci. 124, 1–4, doi:10.1242/jcs.069773 (2011). [PubMed: 21172817]
18. Enninga J, Levay A & Fontoura BM Sec13 shuttles between the nucleus and the cytoplasm and stably interacts with Nup96 at the nuclear pore complex. Molecular and cellular biology 23, 7271–7284, doi:10.1128/mcb.23.20.7271-7284.2003 (2003). [PubMed: 14517296]
19. Mancias JD & Goldberg J Structural basis of cargo membrane protein discrimination by the human COPII coat machinery. EMBO J 27, 2918–2928, doi:10.1038/emboj.2008.208 (2008). [PubMed: 18843296]
20. Lee K et al. HIV-1 Capsid-Targeting Domain of Cleavage and Polyadenylation Specificity Factor 6. J Virol 86, 3851–3860 (2012). [PubMed: 22301135]
21. Gamble TR et al. Crystal structure of human cyclophilin A bound to the amino-terminal domain of HIV-1 capsid. Cell 87, 1285–1294, doi:10.1016/s0092-8674(00)81823-1 (1996). [PubMed: 8980234]
22. Stremlau M, Perron M, Welikala S & Sodroski J Species-specific variation in the B30.2(SPRY) domain of TRIM5alpha determines the potency of human immunodeficiency virus restriction. J. Virol. 79, 3139–3145, doi:10.1128/JVI.79.5.3139-3145.2005 (2005). [PubMed: 15709033]
23. Robinson SB et al. Sequence determinants of the Caenhorhabditis elegans dopamine transporter dictating in vivo axonal export and synaptic localization. Mol Cell Neurosci 78, 41–51, doi:10.1016/j.mcn.2016.11.011 (2017). [PubMed: 27913309]
24. Bajaj Pahuja K et al. Phosphoregulatory protein 14–3-3 facilitates SAC1 transport from the endoplasmic reticulum. Proc Natl Acad Sci U S A 112, E3199–3206, doi:10.1073/pnas.1509119112 (2015). [PubMed: 26056309]
25. Ehrlich LS, Agresta BE & Carter CA Assembly of recombinant human immunodeficiency virus type 1 capsid protein in vitro. J. Virol. 66, 4874–4883 (1992). [PubMed: 1629958]
26. Shah VB & Aiken C In vitro uncoating of HIV-1 cores. Journal of visualized experiments : JoVE, doi:10.3791/3384 (2011).
27. Francis AC, Marin M, Shi J, Aiken C & Melikyan GB Time-Resolved Imaging of Single HIV-1 Uncoating In Vitro and in Living Cells. PLoS Pathog 12, e1005709, doi:10.1371/journal.ppat.1005709 (2016). [PubMed: 27322072]
28. Francis AC & Melikyan GB Single HIV-1 Imaging Reveals Progression of Infection through CA-Dependent Steps of Docking at the Nuclear Pore, Uncoating, and Nuclear Transport. Cell Host Microbe 23, 536–548 e536, doi:10.1016/j.chom.2018.03.009 (2018). [PubMed: 29649444]
29. Dalgleish AG et al. The CD4 (T4) antigen is an essential component of the receptor for the AIDS retrovirus. Nature 312, 763–767, doi:10.1038/312763a0 (1984). [PubMed: 6096719]
30. Klatzmann D et al. T-lymphocyte T4 molecule behaves as the receptor for human retrovirus LAV. Nature 312, 767–768, doi:10.1038/312767a0 (1984). [PubMed: 6083454]
31. Peng K et al. Quantitative microscopy of functional HIV post-entry complexes reveals association of replication with the viral capsid. Elife 3, e04114, doi:10.7554/eLife.04114 (2014). [PubMed: 25517934]
32. Blair WS et al. HIV Capsid is a Tractable Target for Small Molecule Therapeutic Intervention. Plos Pathogens 6, doi:10.1371/journal.ppat.1001220 (2010).
33. Shi J, Zhou J, Shah VB, Aiken C & Whitby K Small-molecule inhibition of human immunodeficiency virus type 1 infection by virus capsid destabilization. Journal of virology 85, 542–549, doi:10.1128/JVI.01406-10 (2011). [PubMed: 20962083]

34. Bester SM et al. Structural and mechanistic bases for a potent HIV-1 capsid inhibitor. Science 370, 360–364, doi:10.1126/science.abb4808 (2020). [PubMed: 33060363]

35. Link JO et al. Clinical targeting of HIV capsid protein with a long-acting small molecule. Nature, doi:10.1038/s41586-020-2443-1 (2020).

References for Online Methods

36. Adachi A et al. Production of acquired immunodeficiency syndrome-associated retrovirus in human and nonhuman cells transfected with an infectious molecular clone. J Virol 59, 284–291 (1986). [PubMed: 3016298]

37. Connor RI, Chen BK, Choe S & Landau NR Vpr is required for efficient replication of human immunodeficiency virus type-1 in mononuclear phagocytes. Virology 206, 935–944, doi:10.1006/viro.1995.1016 (1995). [PubMed: 7531918]

38. Kirmaier A et al. TRIM5 suppresses cross-species transmission of a primate immunodeficiency virus and selects for emergence of resistant variants in the new species. PLoS Biol 8, doi:10.1371/journal.pbio.1000462 (2010).

39. Akiyama H et al. HIV-1 intron-containing RNA expression induces innate immune activation and T cell dysfunction. Nat Commun 9, 3450, doi:10.1038/s41467-018-05899-7 (2018). [PubMed: 30150664]

40. Saenz DT, Barraza R, Loewen N, Teo W & Poeschla EM Feline immunodeficiency virus-based lentiviral vectors. Cold Spring Harb Protoc 2012, 71–76, doi:10.1101/pdb.ip067579 (2012). [PubMed: 22194268]

41. Olsen JC Gene transfer vectors derived from equine infectious anemia virus. Gene Ther 5, 1481–1487, doi:10.1038/sj.gt.3300768 (1998). [PubMed: 9930301]

42. Saenz DT, Teo W, Olsen JC & Poeschla EM Restriction of feline immunodeficiency virus by Ref1, Lv1, and primate TRIM5alpha proteins. J Virol 79, 15175–15188, doi:10.1128/JVI.79.24.15175-15188.2005 (2005). [PubMed: 16306589]

43. Soneoka Y et al. A transient three-plasmid expression system for the production of high titer retroviral vectors. Nucleic Acids Res 23, 628–633, doi:10.1093/nar/23.4.628 (1995). [PubMed: 7899083]

44. Naldini L et al. In vivo gene delivery and stable transduction of nondividing cells by a lentiviral vector. Science 272, 263–267 (1996). [PubMed: 8602510]

45. Morrison JH et al. Feline immunodeficiency virus envelope glycoproteins antagonize tetherin through a distinctive mechanism that requires virion incorporation. J Virol 88, 3255–3272, doi:10.1128/JVI.03814-13 (2014). [PubMed: 24390322]

46. Stremlau M et al. The cytoplasmic body component TRIM5alpha restricts HIV-1 infection in Old World monkeys. Nature 427, 848–853, doi:10.1038/nature02343 (2004). [PubMed: 14985764]

47. de Chaumont F et al. Icy: an open bioimage informatics platform for extended reproducible research. Nat Methods 9, 690–696, doi:10.1038/nmeth.2075 (2012). [PubMed: 22743774]

48. Janas AM & Wu L HIV-1 interactions with cells: from viral binding to cell-cell transmission. Curr Protoc Cell Biol Chapter 26, Unit 26 25, doi:10.1002/0471143030.cb2605s43 (2009).

49. Palmer S et al. Low-level viremia persists for at least 7 years in patients on suppressive antiretroviral therapy. Proc Natl Acad Sci U S A 105, 3879–3884, doi:10.1073/pnas.0800050105 (2008). [PubMed: 18332425]

50. Sharma A et al. A New Class of Multimerization Selective Inhibitors of HIV-1 Integrase. PLoS Pathog. 10, e1004171, doi:10.1371/journal.ppat.1004171 (2014). [PubMed: 24874515]

51. Livak KJ & Schmittgen TD Analysis of relative gene expression data using real-time quantitative PCR and the 2(-Delta Delta C(T)) Method. Methods 25, 402–408, doi:10.1006/meth.2001.1262 (2001). [PubMed: 11846609]

52. Hung M et al. Large-scale functional purification of recombinant HIV-1 capsid. PLoS One 8, e58035, doi:10.1371/journal.pone.0058035 (2013). [PubMed: 23472130]

53. Pornillos O, Ganser-Pornillos BK, Banumathi S, Hua Y & Yeager M Disulfide bond stabilization of the hexameric capsomer of human immunodeficiency virus. Journal of molecular biology 401, 985–995, doi:10.1016/j.jmb.2010.06.042 (2010). [PubMed: 20600115]

54. Perez-Riverol Y et al. The PRIDE database and related tools and resources in 2019: improving support for quantification data. Nucleic Acids Res 47, D442–D450, doi:10.1093/nar/gky1106 (2019). [PubMed: 30395289]
55. Maldonado-Baez L & Wendland B Endocytic adaptors: recruiters, coordinators and regulators. Trends Cell Biol. 16, 505–513, doi:10.1016/j.tcb.2006.08.001 (2006). [PubMed: 16935508]
56. Faini M, Beck R, Wieland FT & Briggs JA Vesicle coats: structure, function, and general principles of assembly. Trends Cell Biol. 23, 279–288, doi:10.1016/j.tcb.2013.01.005 (2013). [PubMed: 23414967]
57. Bethune J, Wieland F & Moelleken J COPI-mediated transport. J. Membr. Biol. 211, 65–79, doi:10.1007/s00232-006-0859-7 (2006). [PubMed: 17041781]
58. Cvitkovic I & Jurica MS Spliceosome database: a tool for tracking components of the spliceosome. Nucleic Acids Res. 41, D132–141, doi:10.1093/nar/gks999 (2013). [PubMed: 23118483]
59. Ibarra A & Hetzer MW Nuclear pore proteins and the control of genome functions. Genes Dev. 29, 337–349, doi:10.1101/gad.256495.114 (2015). [PubMed: 25691464]
60. Ruegsegger U, Beyer K & Keller W Purification and characterization of human cleavage factor Im involved in the 3' end processing of messenger RNA precursors. J. Biol. Chem. 271, 6107–6113, doi:10.1074/jbc.271.11.6107 (1996). [PubMed: 8626397]
61. Nakagawa S, Yamazaki T & Hirose T Molecular dissection of nuclear paraspeckles: towards understanding the emerging world of the RNP milieu. Open Biol 8, doi:10.1098/rsob.180150 (2018).
62. Galganski L, Urbanek MO & Krzyzosiak WJ Nuclear speckles: molecular organization, biological function and role in disease. Nucleic Acids Res. 45, 10350–10368, doi:10.1093/nar/gkx759 (2017). [PubMed: 28977640]
63. Tanaka K The proteasome: overview of structure and functions. Proc Jpn Acad Ser B Phys Biol Sci 85, 12–36, doi:10.2183/pjab.85.12 (2009).
64. Zhou X, Liao WJ, Liao JM, Liao P & Lu H Ribosomal proteins: functions beyond the ribosome. J Mol Cell Biol 7, 92–104, doi:10.1093/jmcb/mjv014 (2015). [PubMed: 25735597]
65. Garrod D & Chidgey M Desmosome structure, composition and function. Biochim. Biophys. Acta 1778, 572–587, doi:10.1016/j.bbamem.2007.07.014 (2008). [PubMed: 17854763]
66. Francis AC, Marin M, Shi J, Aiken C & Melikyan GB Time-Resolved Imaging of Single HIV-1 Uncoating In Vitro and in Living Cells. PLoS Pathog. 12, e1005709, doi:10.1371/journal.ppat.1005709 (2016). [PubMed: 27322072]
67. Kabsch W Xds. Acta crystallographica. Section D, Biological crystallography 66, 125–132, doi:10.1107/S0907444909047337 (2010).
68. McCoy AJ et al. Phaser crystallographic software. J Appl Crystallogr 40, 658–674 (2007). [PubMed: 19461840]
69. Adams PD et al. PHENIX: a comprehensive Python-based system for macromolecular structure solution. Acta Crystallogr. D 66, 213–221, doi:10.1107/S0907444909052925 (2010). [PubMed: 20124702]
70. Afonine PV et al. Towards automated crystallographic structure refinement with phenix.refine. Acta Crystallogr D Biol Crystallogr 68, 352–367, doi:10.1107/S0907444912001308 (2012). [PubMed: 22505256]
71. Emsley P, Lohkamp B, Scott WG & Cowtan K Features and development of Coot. Acta Crystallogr. D 66, 486–501 (2010). [PubMed: 20383002]

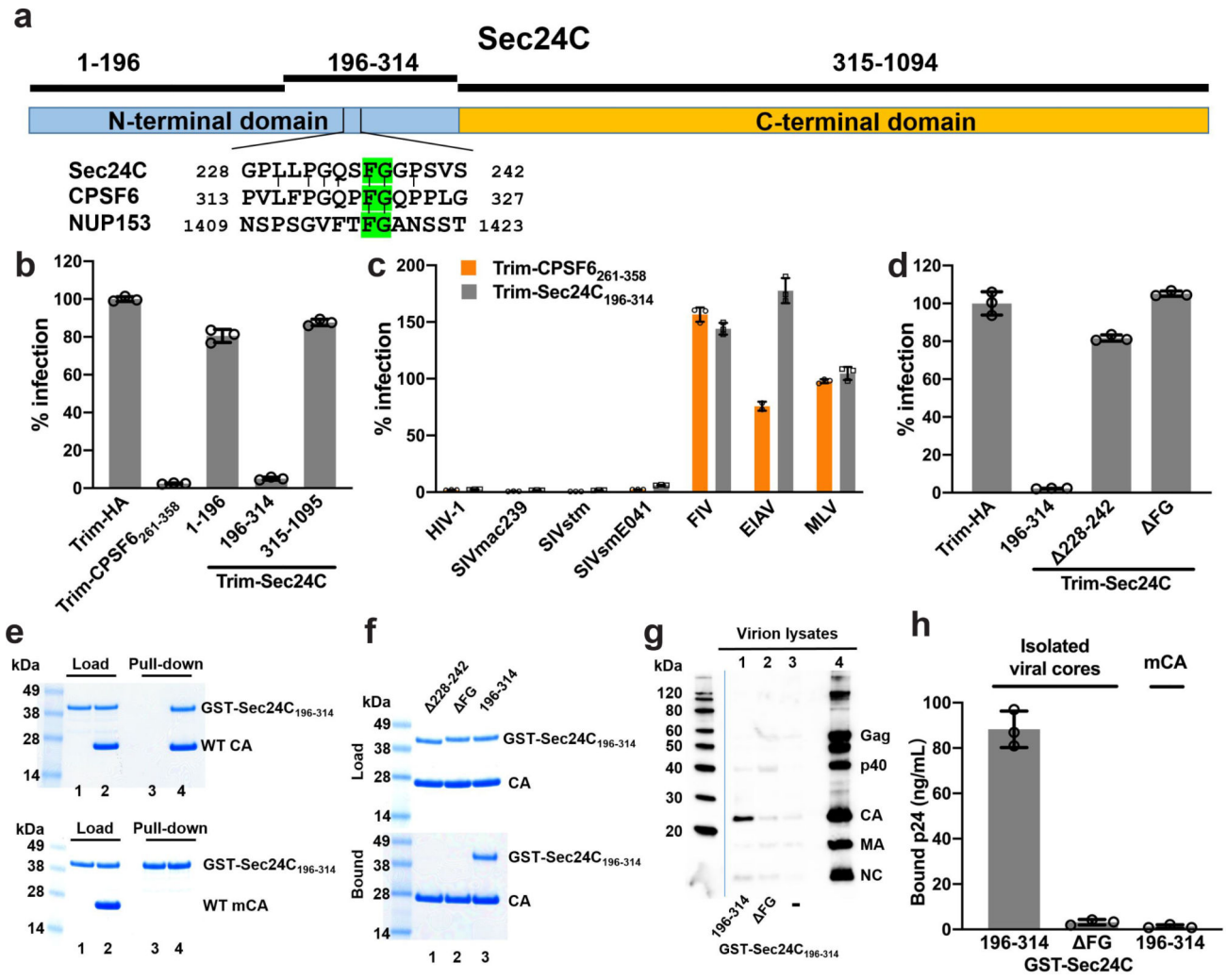

Figure 1. Identification of Sec24C as a cellular interacting partner of HIV-1 cores.

(a) Schematic overview of Sec24C indicating N- and C-terminal domains. The amino acid sequence alignment of the CA-binding FG containing peptide (228–242) of Sec24C with known FG-motifs $CPSF6_{313–327}$ and $Nup153_{1409–1423}$ is shown. Conserved FG residues are highlighted in green. (**b**) Infection levels (normalized to control Trim-HA expressing cells) in HeLa cells stably expressing the indicated Trim-fusion constructs. The normalized and averaged data (+/− SD) from three independent experiments are shown. (**c**) Infection levels (normalized to control Trim-HA expressing cells) of indicated retroviruses in HeLa cells expressing Trim-$Sec24C_{196–314}$ or Trim-$CPSF6_{261–358}$. The normalized and averaged data (+/− SD) from three independent experiments are shown except the data for EIAV infection in Trim-$CPSF6_{261–358}$ expressing HeLa cells are from two independent experiments. (**d**) Infection levels of HIV-1-scarlet in cells stably expressing the indicated Trim-fusions (normalized to control Trim-HA expressing cells). The normalized and averaged data (+/− SD) from three independent experiments are shown. (**e**) Upper panel: representative SDS-PAGE image for pelleting of GST-$Sec24C_{196–314}$ by pre-assembled CA tubes. Lanes 1: load of GST-$Sec24C_{196–314}$ alone; 2: load of GST-$Sec24C_{196–314}$ + WT CA tubes; 3: pelleting of GST-$Sec24C_{196–314}$ alone; 4: pelleting of GST-$Sec24C_{196–314}$ + WT CA tubes. Lower

panel: representative SDS-PAGE image for GST-bead mediated pulldown of GST-Sec24C$_{196–314}$ + monomeric WT CA (WT mCA). Lanes 1: load of GST-Sec24C$_{196–314}$ alone; 2: load of GST-Sec24C$_{196–314}$ + WT mCA; 3: pulldown of GST-Sec24C$_{196–314}$ alone; 4: pulldown of GST-Sec24C$_{196–314}$ + WT mCA. (**f**) Representative SDS-PAGE images for interactions of GST-Sec24C$_{196–314(\Delta 228–242)}$ (lane 1), GST-Sec24C$_{196–314(\Delta FG)}$ (lane 2) and GST-Sec24C$_{196–314}$ (lane 3) with preformed WT CA tubes. Upper and lower gel images show loads and bound fractions, respectively. (**g**) Representative immunoblot using the anti-HIV-1 p55+p24+p17 antibody for pull-down fractions of virion lysates incubated with GST-Sec24C$_{196–314}$ (lane 1), GST-Sec24C$_{196–314(\Delta FG)}$ (lane 2) or pull-down buffer (lane 3). Lane 4: load of virion lysates. (**h**) Quantitative p24 ELISA data for interactions of GST-Sec24C$_{196–314}$ and GST-Sec24C$_{196–314(\Delta FG)}$ with isolated viral cores, and GST-Sec24C$_{196–314}$ with monomeric CA (mCA) isolated from virus lysates by a linear sucrose gradient. The data (mean values +/− SD) from three independent experiments are shown.

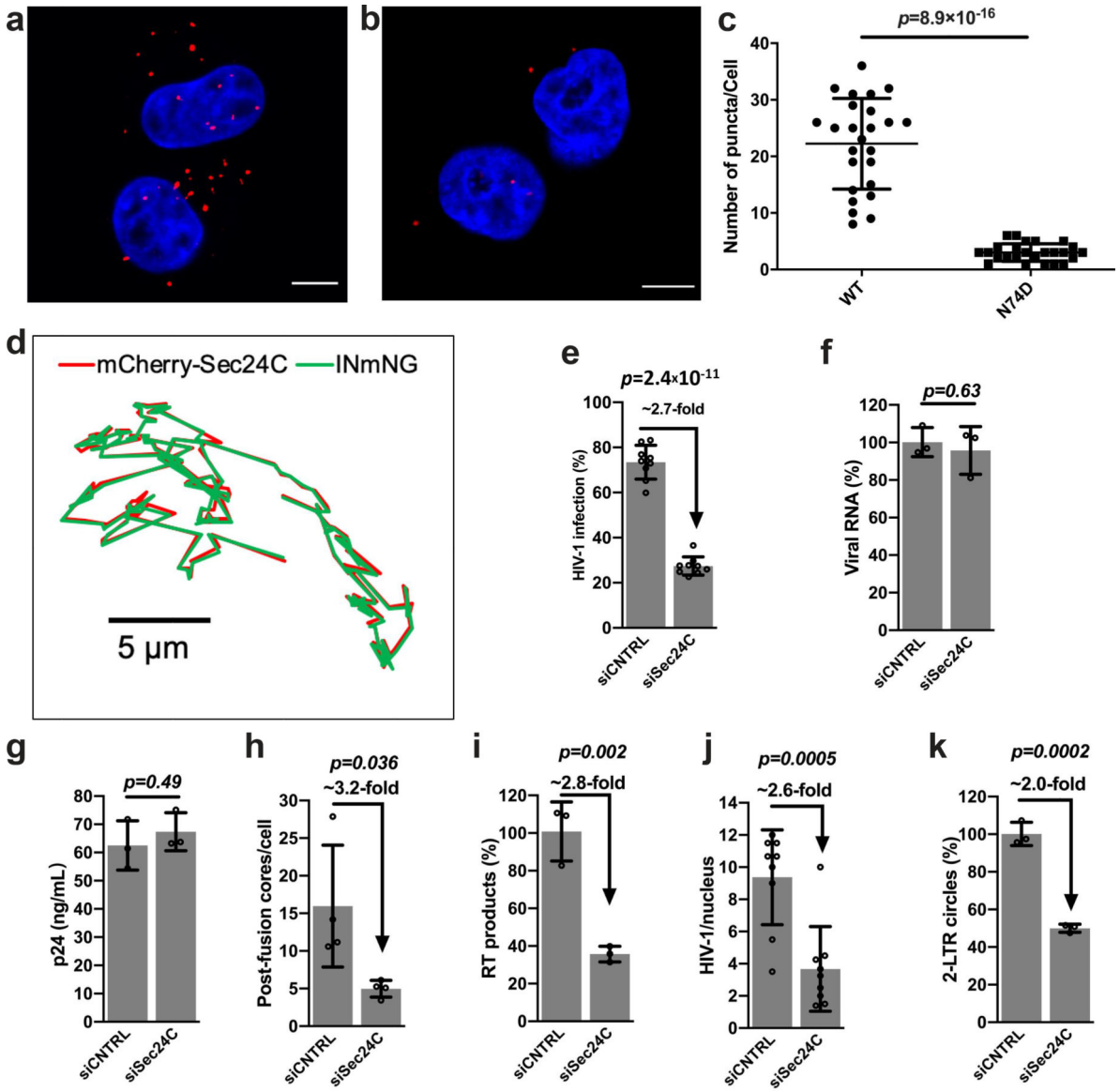

Figure 2. A role of Sec24C during early steps of HIV-1 infection.

(**a-c**) PLA showing association of endogenous Sec24C with incoming HIV-1. HeLa cells were infected with VSV-G pseudotyped HIV-1 harboring WT (**a**) or N74D (**b**) mutant CA. Cells were fixed at 3 hpi, and PLAs were performed using Sec24C and HIV-1 CA specific antibodies. The representative images (**a-b**) show PLA puncta (red) and nuclei stained with DAPI (blue). Scale bar is 5 μm. (**c**) Quantitative results of PLA puncta per cell from analyzing twenty-five cells for each HIV-1 (WT CA) and HIV-1 (CA N74D) infected cells. The data (mean values +/− SD) from three independent experiments are shown. (**d**) Live-cell imaging of single virus co-trafficking with Sec24C. TZM-bl cells transiently expressing the mCherry-Sec24C fusion protein were infected with INmNG-labeled HIVeGFP pseudoviruses and imaged on a Zeiss LSM880 confocal microscope. A representative single virus trajectory corresponding to INmNG and mCherry-Sec24C co-trafficking are shown. (Also see Supplementary Videos 1–3). (**e-k**) The effects of Sec24C depletion on HIV-1

single round infection (**e**) and levels of viral RNA (**f**), p24 (**g**), post-fusion HIV-1 cores (**h**), RT products (**i**), INmNG-labeled HIVeGFP pseudoviruses in the nucleus (**j**) and 2-LTR circles (**k**). The data (mean values +/− SD) from three independent experiments are shown. Statistical significance was determined by two-tailed student *t*-test.

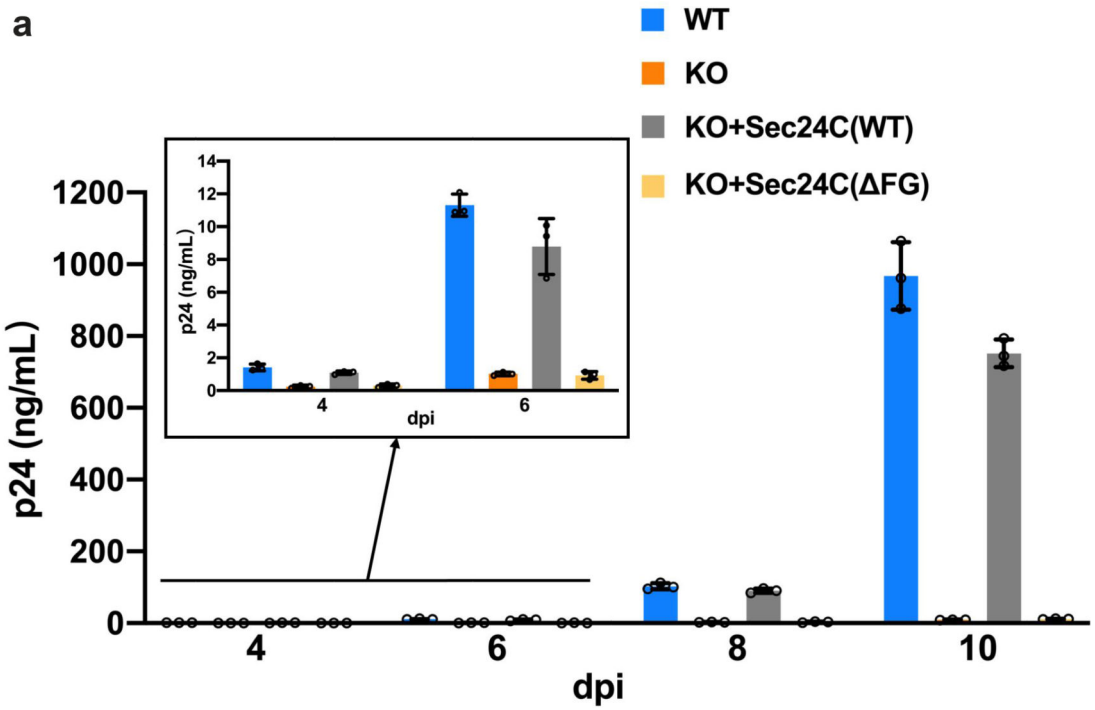

b

Days post infection	Fold-reduction of HIV-1 infection in Sec24C KO cells	*p*-value
4	5.8	0.0008
6	11.1	1.3×10^{-5}
8	38.8	4.1×10^{-5}
10	102.4	6.1×10^{-5}

c

Days post infection	Fold-recovery of HIV-1 infection in KO + Sec24C(WT) cells	*p*-value
4	4.5	0.0004
6	8.6	0.0014
8	34.2	1.3×10^{-5}
10	79.6	4.8×10^{-6}

Figure 3. A role of Sec24C in spreading of replication competent HIV-1 in Jurkat cells.

(**a**) HIV-1_{NL4-3} spread measured by p24 levels in WT (blue graphs), Sec24C KO (orange graphs), KO+Sec24C(WT) (gray graphs) and KO+Sec24C(ΔFG) (yellow graphs) re-expressing (gray line) Jurkat cells. The data (mean values +/− SD) from three independent experiments are shown. Insert: zoomed in view of 4 and 6 dpi results. (**b** and **c**) Quantification of the results in (**a**) to show the fold change and respective *p*-value determined by Student's two-tailed *t*-test for each time point.

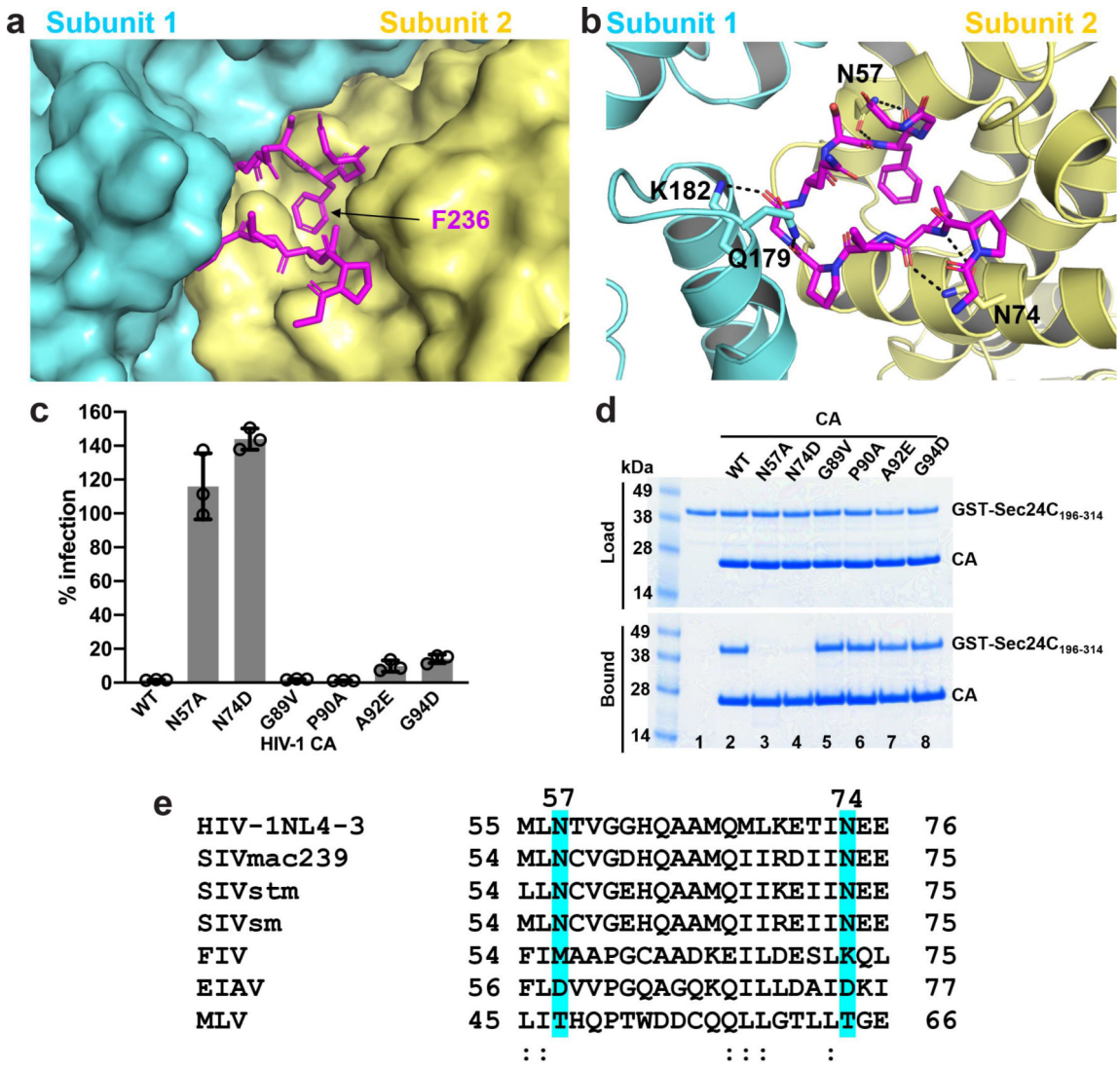

Figure 4. Structural basis for Sec24C$_{228–242}$ interaction with the CA hexamer.

(**a**) X-ray crystal structure of synthetic Sec24C$_{228–242}$ peptides (purple) bound to the CA$_{A14C/E45C/W184A/M185A}$ hexamer with a zoomed in view at the binding pocket formed by adjacent CA subunits 1 (cyan) and 2 (yellow). (**b**) Cartoon representation of the structure indicating interactions between: i) N57 and N74 of CA subunit 2 (yellow) with Sec24C F236 and L230, and ii) CA subunit 1 (cyan) residues K182 and Q179 with Sec24C G233 and P232. (**c**) Infection levels (normalized to infection in control Trim-HA expressing cells) for the indicated HIV-1-scarlet mutant viruses in cells stably expressing Trim-Sec24C$_{196–314}$ were determined by FACS. The data (mean values +/− SD) from three independent experiments are shown. (**d**) Representative SDS-PAGE images for pelleting GST-Sec24C$_{196–314}$ with WT and indicated mutant CA proteins. Upper and lower gel images show loads and bound fractions, respectively. (**e**) Sequence alignments of a Sec24C interacting HIV-1 CA segment with other retroviral CAs.